Master's thesis
Theoretical physics

Trigger efficiency measurement in the charged Higgs boson $H^+ \to \tau_h \nu$ analysis

Mikko Lotti

October 30, 2017

Advisor: Dr. Sami Lehti

Censors: Dr. Sami Lehti
Prof. Kenneth Österberg

UNIVERSITY OF HELSINKI
Department of Physics

PL 42 (Gustaf Hällströmin katu 2)
00014 Helsingin yliopisto

HELSINGIN YLIOPISTO — HELSINGFORS UNIVERSITET — UNIVERSITY OF HELSINKI

Tiedekunta — Fakultet — Faculty	Laitos — Institution — Department
Faculty of Science	Department of Physics

Tekijä — Författare — Author
Mikko Lotti

Työn nimi — Arbetets titel — Title

Trigger efficiency measurement in the charged Higgs boson $H^+ \to \tau_h \nu$ analysis

Oppiaine — Läroämne — Subject
Theoretical physics

Työn laji — Arbetets art — Level	Aika — Datum — Month and year	Sivumäärä — Sidoantal — Number of pages
Master's thesis	October 30, 2017	74

Tiivistelmä — Referat — Abstract

Hiukkasfysiikan standardimalli on yksi nykypäivän tarkimmista teorioista. Vuonna 2012 tapahtuneen Higgsin bosonin havaitsemisen myötä olemme havainneet kaikki alkeishiukkaset ja niiden väliset vuorovaikutukset, jotka standardimalli ennustaa. Tarkkuudestaan huolimatta hiukkasfysiikassa on kuitenkin edelleen ilmiöitä, joita standardimalli ei kykene selittämään. Standardimallin laajennuksiksi kutsutut teoriat pyrkivät selittämään standardimallin avoimia kysymyksiä ja useat laajennukset ennustavat myös uusia hiukkasia. Tämä opinnäytetyö keskittyy kahden-Higgsin-dubletin malleihin joka kuuluu standardimallin laajennuksiin. Nämä mallit ennustavat yhden sijasta yhteensä viisi Higgsin bosonia, joista kaksi on sähköisesti varattuja.

Analyysi, joka on myös esitelty tässä opinnäytetyössä, pyrkii havitsemaan nämä kaksi sähköisesti varattua Higgsin bosonia. Tähän käytetään dataa, joka on kerätty suurella hadronitörmäyttimellä (eng. Large Hadron Collider) käyttäen kompaktia myonisolenoidi-hiukkasilmaisinta (eng. Compact Muon Solenoid). Data kerätään törmäyttämällä protoneita yhteen suurella energialla. Suuri energia mahdollistaa uusien hiukkasten syntymisen ja näitä lopputuotteita tutkimalla voidaan selvittää syntyikö törmäyksessä mahdollisesti eksoottisia, jopa standardimallin ulkopuolisia hiukkasia, kuten sähköisesti varattuja Higgsin bosoneja.

Protonisuihkut törmäävät jopa 40 000 000 kertaa sekunnissa, minkä takia dataa syntyy nopeammin kuin sitä ehditään tallentaa. Tästä syystä tapahtumien lukumäärää on leikattava, mikä tapahtuu käyttämällä liipaisua (eng. trigger system). Liipaisu koostuu hiukkasilmaisimen laitteistoon asennetuista komponenteista sekä laitteiston ulkopuolisista tietokoneohjelmistoista, jotka päättävät mitä osia kerätystä datasta on syytä tallentaa. Liipaisu on suunniteltu niin, että valinnan läpäisevät esimerkiksi hyvin energeettiset hiukkaset, jotka saattavat olla lähtöisin mielenkiintoisista kohteista. Liipaisun jälkeen datan määrä on vähentynyt niin että se on mahdollista kirjoittaa levylle tallennusta varten.

Tässä opinnäytetyössä esitän uuden menetelmän mitata liipaisun tehokkuutta. Tehokkuus määritellään liipaisun valintaan sisään tulevien hiukkasten ja valinnan läpäisseiden hiukkasten lukumäärien suhteena. Uusi menetelmä sovittaa mitattuun ja simuloituun liipaisun tehokkuuteen funktion ja näin vähentää tehokkuuden mittauksen systemaattista epävarmuutta. Tämä pienentää koko analyysin systemaattisia virhelähteitä ja parantaa lopullisia tuloksia.

Avainsanat — Nyckelord — Keywords
charged Higgs boson

Säilytyspaikka — Förvaringsställe — Where deposited

Muita tietoja — övriga uppgifter — Additional information

Contents

1. Introduction

In 2012 Compact Muon Solenoid (CMS) and a toroidal LHC apparatus (ATLAS) detectors at Large Hadron Collider (LHC) pronounced the discovery of a Higgs boson [12] [8]. The discovery of this scalar boson meant that the theory of particles and their interactions, the Standard Model, was complete. We have now observed all the particles predicted by the Standard Model and we've not yet detected any particles that are not part of it.

Although successful, the Standard Model has some problems. For example the particles in the Standard Model make in total only five percent of our universe. Dark matter and dark energy make the rest 95 % but the Standard Model doesn't give a candidate for this matter. To overcome these obstacles, various extensions of the Standard Model are being studied.

The discovery of an additional scalar boson would be an evidence of an extended Higgs sector. An extended scalar sector can be constructed by introducing a second scalar doublet to the Standard Model. These models are called two-Higgs-doublet-models [35] and they are considered in this thesis. The model predicts in total five Higgs bosons: one neutral Higgs boson h, another heavier neutral Higgs boson H, a pseudoscalar A, and two charged Higgs bosons $H^{\pm}$. The two-Higgs-doublet-models are also the first step towards more sophisticated theories such as the Supersymmetry [44] [43], which would predict even more particles and give possible solutions to the problems of the Standard Model such as a candidate for dark matter.

Experiments have been conducted trying to observe these beyond the Standard Model Higgs bosons, and experimental limits have been extracted from the data. At the Large Electron-Positron collider a 78.6 GeV lower limit has been set at a 95 % confidence level to the charged Higgs boson mass [3]. Upper limits for the production of the charged Higgs boson have been set at the CMS [13] and ATLAS [2] experiments. Also at Fermilab, D0 [19] and CDF [9] experiments have studied the upper limits of the production.

This thesis is focused on the analysis trying to find the charged Higgs bosons at the CMS detector. We compare the prediction of the Standard Model to data and try to see if the predictions are true. Possible excess in the data could be an evidence of a charged Higgs bosons and beyond the Standard Model theories.

The first step of any analysis is the trigger. The trigger system is needed in the experiments to select interesting events potentially containing new physics [15]. The trigger selection happens at the same time together with the particle collisions. The main goal of this work was to implement a new method to measure the efficiency of the trigger used in the charged Higgs boson analysis. As the most dominant sources of systematical uncertainties in the analysis come from the trigger, more accurate method would increase the accuracy of the whole analysis.

2. The Standard Model and the Higgs mechanism

The Standard Model (SM) is a theory of particles and interactions which are described with quantum fields. Particles are excitations of these fields and quantum field theories give us the tools to calculate the properties of the particles and their interactions. The SM describes all matter on Earth by point-like spin 1/2 fermions. Although successful, the SM doesn't seem to describe everything we observe in space: baryon antibaryon asymmetry and the formation of galaxies which could be described with cold dark matter. There are in total four fundamental forces in nature: electromagnetic, weak interaction, strong interaction and gravity. The SM describes first three of these. The forces are meditated by gauge bosons, a spin 1 particles. There is also a spin zero boson included in the SM, the Higgs boson.

In the following sections we will see how the Standard Model is formulated. We will use the gauge principle to discover the allowed interactions and see the wide range of SM particles. The major parts of the SM are gauge invariance and renormalizibility. With these tools we can describe the forces and particles that surround us on Earth.

2.1 Particle content and the gauge group

The Standard Model has in total of 17 particles that describe matter and forces: 6 quarks, 6 leptons, 4 gauge bosons and the Higgs boson. Quarks and leptons are fermions. Fermions are particles with a half integer spin and they obey Fermi-Dirac statistics. Leptons, for instance electrons, are free particles, but quarks are confined into bound states, as quarks interact through strong interaction. These bound states are for example protons and neutrons which are called baryons. Quarks can also form bound states called mesons where two quarks, a quark and an antiquark, are bound together. Quarks and leptons are categorised by their properties to three families.

The gauge symmetry group of the Standard Model is $\mathrm{SU}(3)_c \times \mathrm{SU}(2)_L \times \mathrm{U}(1)_Y$. Everyone of these algebras have generators, which correspond to a specific gauge

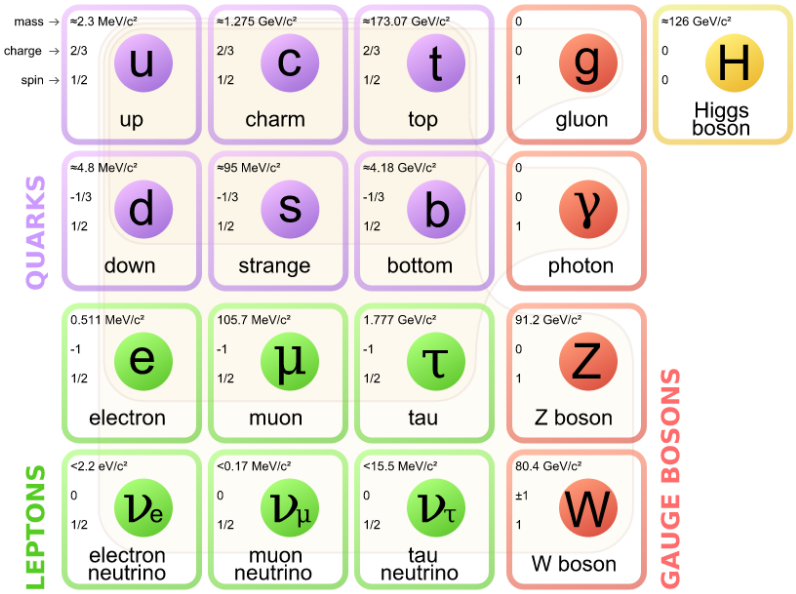

Figure 2.1: The family structure of the Standard Model [37].

boson. For U(1) we have one photon, for SU(2) W^+, W^- and Z bosons and for SU(3) eight gluons. Photons govern the electricity and magnetism. If we describe this with quantum field theories, this brings out the Quantum Electrodynamics (QED). If we add the weak interaction to the QED we get the Electroweak Theory SU(2)×U(1). Weak interaction is seen for example in radioactive decays such as beta decay. For instance, it makes it possible for a neutron to transform into a proton by emitting an electron and an antineutrino. Strong interaction is described by Quantum Chromodynamics (QCD) where gluons bind together quarks to form hadrons.

The subscripts indicate the quantum number carried by the gauge group. The subscript "c" stands for colour, referring to the bound states of quarks. The subscript "L" indicates that only the left-handed fermions carry this quantum number. And "Y" stands for weak hypercharge, which is associated with the familiar electric charge.

2.2 Quantum electrodynamics and gauge invariance

Quantum Electrodynamics (QED) describes how light and matter interact. QED is based on the U(1) gauge invariance which gives arise to a photon, a massless spin 1 gauge boson. To see this, we consider the Dirac Lagrangian, which is used to describe the physics of our system:

$$\mathcal{L}_{Dir} = i(\bar{\psi}\gamma^{\mu}\partial_{\mu}\psi) - m\bar{\psi}\psi = \bar{\psi}(i\partial\!\!\!/ - m)\psi. \tag{2.1}$$

The Dirac Lagrangian is invariant under U(1) symmetry group which is equivalent of a rotation in the complex plane. By constructing Lagrangians that are U(1) invariant, we demand that the physics of the system stay the same even if we rotate it.

We can do the rotation for the fields ψ

$$\begin{aligned} \psi \rightarrow \psi' &= e^{-iq\alpha}\psi \\ \bar{\psi} \rightarrow \bar{\psi}' &= e^{iq\alpha}\psi, \end{aligned} \tag{2.2}$$

where q and α are constants. The transformation is global when the factor α remains a constant.

By substituting the transformed fields 2.2 to the Dirac Lagrangian 2.1, we can see that the Lagrangian is in fact invariant under this transformation.

$$\begin{aligned} \mathcal{L}_{Dir} \rightarrow \mathcal{L}'_{Dir} &= e^{iq\alpha}\bar{\psi}(i\partial\!\!\!/ - m)e^{-iq\alpha}\psi \\ &= e^{iq\alpha}e^{-iq\alpha}\bar{\psi}(i\partial\!\!\!/ - m)\psi \\ &= \bar{\psi}(i\partial\!\!\!/ - m)\psi \\ &= \mathcal{L}_{Dir} \end{aligned} \tag{2.3}$$

What happens when the alpha is not constant but is actually dependent on the space-time coordinate x? The transformation is now called local:

$$\begin{aligned} \psi \rightarrow \psi' &= e^{-iq\alpha(x)}\psi \\ \bar{\psi} \rightarrow \bar{\psi}' &= e^{iq\alpha(x)}\psi. \end{aligned} \tag{2.4}$$

Using 2.4 to 2.1 we can see that the local transformation doesn't seem to leave the Lagrangian invariant:

$$\begin{aligned}\mathcal{L}_{Dir} \to \mathcal{L}'_{Dir} &= e^{iq\alpha(x)}\bar{\psi}(i\not{\partial} - m)e^{-iq\alpha(x)}\psi \\ &= e^{iq\alpha(x)}e^{-iq\alpha(x)}\bar{\psi}(i\not{\partial} - m)\psi - \bar{\psi}(i^2 q\gamma^\mu\psi\partial_\mu\alpha(x)) \\ &= \mathcal{L}_{Dir} + q\bar{\psi}\gamma^\mu\psi\partial_\mu\alpha(x), \end{aligned} \tag{2.5}$$

due to this extra term appearing. This problem can be tackled by introducing a transformation in the derivative. We call this the covariant derivative:

$$\partial_\mu \to D_\mu = \partial_\mu + iqA_\mu, \tag{2.6}$$

but by doing this transformation, the field itself must transform as well:

$$A_\mu \to A'_\mu = A_\mu + \partial_\mu\alpha(x). \tag{2.7}$$

Now if we perform the local transformation 2.2 together with the covariant derivative 2.6 and the field transformation 2.7 to the Dirac Lagrangian 2.1

$$\begin{aligned}\mathcal{L}_{Dir} \to \mathcal{L}'_{Dir} &= e^{iq\alpha(x)}\bar{\psi}(i\not{D}_\mu - m)e^{-iq\alpha(x)}\psi \\ &= e^{iq\alpha(x)}\bar{\psi}(i\gamma^\mu\partial_\mu e^{-iq\alpha(x)} - \gamma^\mu qA'_\mu e^{-iq\alpha(x)} - me^{-iq\alpha(x)})\psi \\ &= e^{iq\alpha(x)}e^{-iq\alpha(x)}\bar{\psi}(i\not{\partial} - i^2 q\gamma^\mu\partial_\mu\alpha(x) - \gamma^\mu qA_\mu - q\gamma^\mu\partial_\mu\alpha(x) - m)\psi \\ &= \bar{\psi}(i\not{\partial} + q\gamma^\mu\partial_\mu\alpha(x) - \gamma^\mu qA_\mu - q\gamma^\mu\partial_\mu\alpha(x) - m)\psi \\ &= \bar{\psi}(i\not{\partial} - m)\psi - q\bar{\psi}\gamma^\mu\psi A_\mu \\ &= \mathcal{L}_{Dir} - q\bar{\psi}\gamma^\mu\psi A_\mu \qquad (2.8) \\ &= \mathcal{L}_{Dir} + \mathcal{L}_{int} \qquad (2.9)\end{aligned}$$

This new interaction term in the Lagrangian 2.8 corresponds to the coupling of two fermions to a photon. The constant value in front corresponds to the strength of the coupling or the vertex of the Feynman graph as seen in Fig. 2.2. By demanding the invariance of the Lagrangian we've predicted an interaction, this is called the gauge principle and we will exploit it in the following sections.

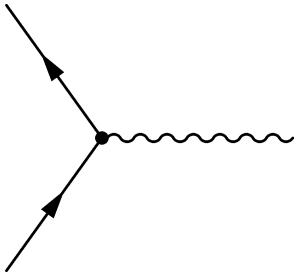

Figure 2.2: QED interaction: coupling of two fermions to a photon

The Lagrangian of QED is still not complete. It still lacks the description of photons, which we know as magnetic and electric fields. The Lagrangian of these interactions is

$$\mathcal{L}_\gamma = -\frac{1}{4}F^{\mu\nu}F_{\mu\nu}. \tag{2.10}$$

Here $F_{\mu\nu}$ is the electromagnetic tensor

$$F_{\mu\nu} = \partial_\mu A_\nu - \partial_\nu A_\mu. \tag{2.11}$$

With the electromagnetic tensor we can describe all the Maxwell's equations in a simpler form.

By adding this Lagrangian to the QED Lagrangian we allow the photons to propagate.

$$\mathcal{L}_{QED} = \mathcal{L}_{Dir} + \mathcal{L}_{int} + \mathcal{L}\gamma \tag{2.12}$$

$$\mathcal{L}_{QED} = \bar{\psi}(i\partial\!\!\!/ - m)\psi - q\bar{\psi}\gamma^\mu A_\mu\psi - \frac{1}{4}F^{\mu\nu}F_{\mu\nu} \tag{2.13}$$

From this Lagrangian we can see that leptons share the same coupling strength q with a photon. The electric charge determines the interaction strength and q is in fact the electric charge $q = e$ of the lepton which is same for electrons, muons and taus.

2.3 Weak interaction and the electroweak unification

The weak interaction is mediated by massive vector bosons. Probably the most familiar effect of the weak force is the beta decay. This nuclear reaction makes for instance fusion and fission possible. The changing of hadrons into other hadrons is possible through weak interaction, where one quark changes to another through exchange of a W boson.

It was experimentally detected that a kaon decays rarely into a final state with two pions [7]. This means that for some reason an CP-odd state decays into an CP-even state, and breaks CP invariance, the conservation of charge conjugation parity symmetry. This behavior can be explained through complex phases appearing in the theory. CP-transformation loosely corresponds to the change of a particle to its antiparticle and this violation could be responsible for the baryon asymmetry in the universe which is still one of the unanswered question of the SM.

The observed behavior leads to introducing new properties to particles such as fermionic flavours and different properties for left and right handed fields. The left handed fermions appear as doublets and carry SU(2) indices but right-handed singlets don't transform under SU(2). This leads to a situation where only left handed fermions and right handed antifermions couple to the $W^{\pm}$. To describe all this we need more difficult algebra. We need a new group SU(2) that describes the doublet structure which demands that the gauge transformations don't commute. This means we can't anymore trivially change the order of operators in our calculations. We call such theories non-abelian.

In order to take into account the difference between the left and right-handed fermions, we introduce them as two separate fields:

$$\psi = \psi_R + \psi_L. \tag{2.14}$$

Through this we can separate the Lagrangian to left and right handed components as well:

$$\mathcal{L} = \mathcal{L}_R + \mathcal{L}_L \tag{2.15}$$

$$\rightarrow \mathcal{L} = \bar{\psi}_L(i\partial\!\!\!/ - m)\psi_L + \bar{\psi}_R(i\partial\!\!\!/ - m)\psi_R. \tag{2.16}$$

Now we must also sum over all fermion generations:

$$\psi_{L1} = \begin{pmatrix} \nu_e \\ e \end{pmatrix}_L, \psi_{L2} = \begin{pmatrix} \nu_\mu \\ \mu \end{pmatrix}_L, \psi_{L3} = \begin{pmatrix} \nu_\tau \\ \tau \end{pmatrix}_L, \tag{2.17}$$

$$\psi_{R1} = e_R, \psi_{R2} = \mu_R, \psi_{R3} = \tau_R. \tag{2.18}$$

The right handed neutrino singlet doesn't appear as we've not detected right handed neutrinos so far. The antiparticle of a left handed particle is an adjoint of a right handed particle. This way the theory has a built-in property that the left-handed leptons couple to neutrinos but there are no interactions between right-handed leptons and neutrinos.

As we've formulated the basis of the new part of our theory, we are motivated to use the gauge principle to find all the interactions. In a non-abelian gauge theory A_μ gets promoted to a matrix:

$$A_\mu \to A_\mu = A_\mu^a \frac{\sigma^a}{2} \tag{2.19}$$

Here σ^a are the generators of SU(2) or more familiarly the Pauli matrices. The number of generators is the same as the dimension of the group. For SU(N) the dimension is $\mathrm{Dim(SU(N))} = N^2 - 1$ which gives us three generators in the case of SU(2). The three generators correspond to gauge bosons in the theory. We saw this in the case of U(1) in QED, where the one generator led to one vector field A_μ.

Now the fields transforms as

$$\psi \to V\psi \tag{2.20}$$

$$\bar{\psi} \to \bar{\psi}V^\dagger \tag{2.21}$$

where V is SU(2) matrix. $V = e^{i\frac{\sigma^a}{2}}$. It only acts on the doublet field as it is the only field carrying the correct indices to perform the contraction with. As a special unitary matrix, the V obeys $VV^\dagger = 1$ and $\det(V) = 1$

We make a local transformation to the Lagrangian to see how it behaves.

$$\mathcal{L} \to \mathcal{L}' = \bar{\psi}_i V^\dagger(x)(i\partial\!\!\!/ - m_i)V(x)\psi_i \tag{2.22}$$

$$= \bar{\psi}_i(i\partial\!\!\!/ - m_i)\psi_i + i\bar{\psi}_i V^\dagger(\partial\!\!\!/ V)\psi_i. \tag{2.23}$$

Here we dropped the explicit dependence on the space-time coordinate x but the

transform is still local. We must again demand local gauge invariance so the covariant derivative becomes:

$$D_\mu = \partial_\mu \mathbf{1} + igA_\mu \tag{2.24}$$

and follow the usual procedure and transform the gauge field as well

$$A_\mu \to VA_\mu V^\dagger + \frac{i}{g} V^\mu \partial_\mu V^\dagger \tag{2.25}$$

To check that these expressions are consistent, we can insert the covariant derivative and the field transformation to 2.23.

$$\begin{aligned}
\mathcal{L}' &= \bar{\psi}_i(i\not{D} - m_i)\psi_i && (2.26)\\
&= \bar{\psi}_i(i\not{\partial} - m_i)\psi_i + i\bar{\psi}_i V^\dagger(\not{\partial}V)\psi_i + ig\bar{\psi}_i V^\dagger V\gamma^\mu A_\mu V^\dagger V\psi_i && (2.27)\\
&\quad - i\bar{\psi}_i V^\dagger V V^\dagger(\not{\partial}V)V^\dagger V\psi_i && (2.28)\\
&= \bar{\psi}_i(i\not{\partial} + i\gamma^\mu g A_\mu - m_i)\psi_i && (2.29)\\
\to \mathcal{L} &= \mathcal{L}' && (2.30)
\end{aligned}$$

From this we can see that the covariant derivative was chosen correctly as it stays invariant in the transformation.

Now we want to write down the covariant derivative explicitly, as it will help us in the next section and describe the electroweak unification: the situation where the three gauge bosons of weak interaction couple to the leptons of the QED. First we need to define the weak isospin operators:

$$\tau^1 = \frac{1}{2}\begin{pmatrix} 0 & 1 \\ 1 & 0 \end{pmatrix}, \tau^2 = \frac{1}{2}\begin{pmatrix} 0 & -i \\ i & 0 \end{pmatrix}, \tau^3 = \frac{1}{2}\begin{pmatrix} 1 & 0 \\ 0 & -1 \end{pmatrix} \tag{2.31}$$

which satisfy the commutation relation

$$[\tau^a, \tau^b] = i\epsilon_{abc}\tau^c. \tag{2.32}$$

The weak isospin is the "charge" of the weak interaction that tells how the particles interact with each other. We define the operators τ^i so that $\tau^i = \frac{\sigma^i}{2}$, where σ^i are

the Pauli matrices. With the weak isospin operators the covariant derivative gets the form:

$$D_\mu = \partial_\mu \mathbf{1} + igW_\mu^i \tau_i = \begin{pmatrix} \partial_\mu + \frac{ig}{2}W^3 & \frac{ig}{2}(W^1 - iW^2) \\ \frac{ig}{2}(W^1 + iW^2) & \partial_\mu - \frac{ig}{2}W^3 \end{pmatrix} \tag{2.33}$$

Now we want to include the U(1) hypercharge interaction. We do it by performing a local SU(2)×U(1) transformation:

$$U = e^{i\omega^a(x)\tau_a} e^{iY\alpha(x)}, \tag{2.34}$$

where the factor Y describes the weak hypercharge, which is defined as:

$$Q = \tau^3 + Y \tag{2.35}$$
$$\rightarrow Y = (Q - \tau^3). \tag{2.36}$$

Here Q is the familiar electric charge and τ^3 is the third weak isospin operator appearing in 2.31, or the third component of weak isospin.

Now the Lagrangian transforms:

$$\mathcal{L} = \bar{\psi}U^\dagger(i\partial\!\!\!/ - m)U\psi \tag{2.37}$$
$$= \bar{\psi}(i\partial\!\!\!/ - m)\psi + i\omega^a\bar{\psi}(\partial\!\!\!/\tau_a)\psi + iY\bar{\psi}(\partial\!\!\!/\alpha)\psi \tag{2.38}$$

Yet again we demand the local gauge invariance so the covariant derivative becomes:

$$D_\mu = \partial_\mu + igW_\mu\tau_i + ig'YB_\mu \tag{2.39}$$

where W is responsible for SU(2) and has three components, and B describes the U(1).

The gauge field W and the new field B transform as well

$$W_\mu \rightarrow W'_\mu = e^{i\omega^a\tau_a}W_\mu e^{-i\omega^a\tau_a} + \frac{i}{g}(\partial_\mu e^{i\omega^a\tau_a})e^{-i\omega^a\tau_a} \tag{2.40}$$

$$B_\mu \rightarrow B'_\mu = B_\mu + \frac{iY}{g'}\partial_\mu\alpha. \tag{2.41}$$

Finally we write the covariant derivative explicitly with the help of operators τ^a:

$$D_\mu = \partial_\mu \mathbf{1} + igW_\mu^i \tau_i + ig'YB_\mu = \begin{pmatrix} \partial_\mu + \frac{ig}{2}W_\mu^3 + ig'YB_\mu & \frac{ig}{2}(W_\mu^1 - iW_\mu^2) \\ \frac{ig}{2}(W_\mu^1 + iW_\mu^2) & \partial_\mu - \frac{ig}{2}W_\mu^3 + ig'YB_\mu \end{pmatrix} \tag{2.42}$$

We have now generated a matrix that describes the weak interaction: the diagonal elements describe the neutral currents and the off-diagonal elements describe the charged currents. These so-called currents describe interactions where either positive or negative charge flows or a neutral Z boson interacts. We can now also see the reason why we use the notation $\mathrm{SU}(2)_L$: only left-handed fields are affected by the SU(2) part of the transformation but both right- and left-handed fields are affected by the U(1) part. We have now combined the QED described by $\mathrm{U}(1)_Y$ and weak interaction described by $\mathrm{SU}(2)_L$ into combined symmetry $\mathrm{SU}(2)_L \times \mathrm{U}(1)_Y$. This is called the electroweak unification.

The masses of the W and the Z bosons have been measured to be 80.385 GeV and 91.188 GeV, but there appears no mass terms in the Lagrangian. Because of the gauge principle, we can't just add additional mass terms to the system. We also can't put away the gauge invariance as the whole theory becomes non-renormalizable. To reflect the experimental findings, Guralnik, Hagen and Kibble [31], Brout and Englert [24] and Higgs [34] separately formulated a mechanism to generate masses for W and Z. This happens through symmetry breaking and is usually called the Higgs mechanism. We will discuss this mechanism in Section 2.5.

2.4 Quantum chromodynamics

Quantum chromodynamics (QCD) is the theory of strong interactions, describing the interactions between quarks and gluons. The interaction particle gluon, a spin 1 massless boson, is the generator of this interaction. Gluons bind quarks together to form hadrons. Like weak interaction, the strong interaction is described with a non-abelian gauge theory and therefore the operators, describing the fields, don't commute. Although the strong interaction shares same kind of properties as the weak interaction through the behavior of non-abelian theory, there is a difference between the two; the force of strong interaction is large at large distances.

It was proposed [32] that quarks carry additional, unobserved quantum number. Later this got the name colour. This colour charge is useful as it defines the local symmetry meaning that we must add another index to our theory. There are in total three colours, red (r), green (g) and blue (b), and their anticolours, but we observe combinations of these three colour in such a way that the end result is colourless. We say that sum of r g b is colourless and sum of colour and its anticolour is

also colourless. All mesons and baryons are colourless and therefore we call this the colour confinement. Due to this confinement we can have only two types of hadrons: baryons with three quarks or mesons with two.

This means, that the six quarks of the SM, which are described with four-component Dirac spinors carry now also the index of colour. After this we can describe quarks with colour triplets with respect to SU(3).

$$q = \begin{pmatrix} q_r \\ q_g \\ q_b \end{pmatrix} \tag{2.43}$$

As stated, QCD is a non-abelian gauge theory, and non-abelian theories are asymptotically free. In the case of SU(3), the running of the coupling constant α_s also behaves differently at small distances compared to weak interaction. At large distances (small energies), the constant is large, which means that quarks are bound to be in hadrons. But as the energy grows, α_s gets weaker meaning that the particles are almost noninteracting. This is called the asymptotic freedom.

Now we are using SU(3) to describe the strong interaction and like earlier, the generators of SU(3) are responsible for the physical gluons. There are in total eight generators and thus eight gluons. We had the Pauli matrices in the SU(2) case, but in the SU(3) the generators are called the Gell-Mann matrices:

$$\lambda_1 = \begin{pmatrix} 0 & 1 & 0 \\ 1 & 0 & 0 \\ 0 & 0 & 0 \end{pmatrix}, \lambda_2 = \begin{pmatrix} 0 & -i & 0 \\ i & 0 & 0 \\ 0 & 0 & 0 \end{pmatrix}, \lambda_3 = \begin{pmatrix} 1 & 0 & 0 \\ 0 & -1 & 0 \\ 0 & 0 & 0 \end{pmatrix}, \tag{2.44}$$

$$\lambda_4 = \begin{pmatrix} 0 & 0 & 1 \\ 0 & 0 & 0 \\ 1 & 0 & 0 \end{pmatrix}, \lambda_5 = \begin{pmatrix} 0 & 0 & -i \\ 0 & 0 & 0 \\ -i & 0 & 0 \end{pmatrix}, \lambda_6 = \begin{pmatrix} 0 & 0 & 0 \\ 0 & 0 & 1 \\ 0 & 1 & 0 \end{pmatrix}, \tag{2.45}$$

$$\lambda_7 = \begin{pmatrix} 0 & 0 & 0 \\ 0 & 0 & -i \\ 0 & i & 0 \end{pmatrix}, \lambda_8 = \frac{1}{\sqrt{3}} \begin{pmatrix} 1 & 0 & 0 \\ 0 & 1 & 0 \\ 0 & 0 & -2 \end{pmatrix} \tag{2.46}$$

Again we want to perform the gauge transformation and in the SU(3) case the transformation is

$$q \to q' = Uq \tag{2.47}$$

$$\bar{q} \to \bar{q} = U^\dagger \bar{q} \tag{2.48}$$

Then the covariant derivative becomes:

$$\partial_\mu \rightarrow D_\mu = \partial_\mu + ig_s \mathbf{G}_\mu \tag{2.49}$$

And finally, the field transforms as well:

$$G_\mu = UG_\mu U^\dagger + \frac{i}{g_s}(\partial U)U^\dagger \tag{2.50}$$

This is all very similar to the weak interaction case. In the end QCD Lagrangian gets the form:

$$\begin{aligned}
\mathcal{L}_{QCD} &= -\frac{1}{2}Tr(G^{\mu\nu}G_{\mu\nu}) + \bar{q}(i\gamma^\mu D_\mu - m_q)q \qquad (2.51)\\
&= -\frac{1}{4}(\partial^\mu G^\nu_a - \partial^\nu G^\mu_a)(\partial_\mu G^a_\nu - \partial_\nu G^a_\mu) + \sum_q \bar{q}_\alpha(i\gamma^\mu\partial_\mu - m_q)q_\alpha \\
&+ \frac{1}{2}\sum_q g_s(\bar{q}_\alpha(\lambda^a)_{\alpha\beta}\gamma^{mu}q_\beta)G^a_\mu \\
&- \frac{1}{2}g_s f_{abc}(\partial_\mu G^a_\nu - \partial_\nu G^a_\mu)G^\mu_b G^\nu_c \\
&- \frac{1}{4}g_s^2 f_{abc}f_{ade}G^\mu_b G^\nu_c G^d_\mu G^e_\nu \qquad (2.52)
\end{aligned}$$

From the three last terms one can read the couplings of gluons with fermions and two kinds of self coupling among gluons: 3 and 4 self interactions.

2.5 Spontaneous symmetry breaking and the Higgs mechanism

The mechanism needed to generate masses for Z and W bosons is called spontaneous symmetry breaking (SSB), where the SU(2) × U(1) symmetry gets broken. In SSB the Lagrangian is symmetric, or invariant, under a transformation, but the ground state, describing the minimum of the system, is not. We can break the symmetry by expanding the state around a minimum and we say that the breaking is spontaneous as it does not happen by external reasons.

Now we want to break the electroweak symmetry. For this we need to introduce a

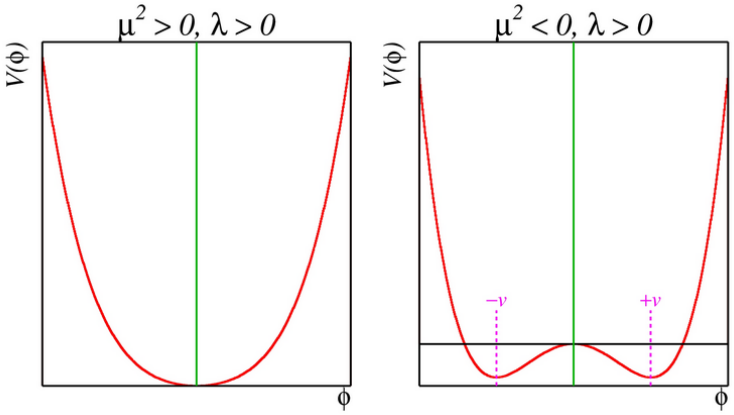

Figure 2.3: Potential of the scalar field for different parameters.

new scalar SU(2) doublet:

$$\Phi = \begin{pmatrix} \phi^+ \\ \phi^0 \end{pmatrix}. \tag{2.53}$$

Both elements ϕ_0 and ϕ^+ are complex scalars. The Lagrangian for the scalar field is

$$\mathcal{L}_{scalar} = \partial_\nu \Phi^\dagger \partial^\nu \Phi - \mu^2 \Phi^\dagger \Phi - \lambda (\Phi^\dagger \Phi)^2. \tag{2.54}$$

We wish to minimize the potential term of this scalar Lagrangian. The minimum of the potential can be found with

$$\frac{\partial V}{\partial \Phi^\dagger} = \mu^2 \Phi + 2\lambda \Phi^\dagger \Phi^2 = 0. \tag{2.55}$$

Next we will allow the mass (or the minimum) to be negative $\mu^2 < 0$, which gives us the so-called Mexican hat potential like on the right hand side in Figure 2.3 as there appears a maximum in $\phi = 0$. The minimum is now

$$\Phi^\dagger\Phi = \phi^{+\dagger}\phi^+ + \phi_0^\dagger\phi_0 \tag{2.56}$$

$$= -\frac{\mu^2}{2\lambda} \tag{2.57}$$

$$\Rightarrow \phi^0 = 0 \tag{2.58}$$

$$\phi^+ = \sqrt{-\frac{\mu^2}{2\lambda}} = v/\sqrt{2} \tag{2.59}$$

$$\Leftrightarrow \Phi = \begin{pmatrix} 0 \\ v/\sqrt{2} \end{pmatrix} \tag{2.60}$$

Here the symmetry has been broken spontaneously, as the state is at the nonsymmetric minimum. It follows from the Goldstone theorem, that for each broken symmetry a massless state will appear [29].

We demand that the Lagrangian is still invariant before the SSB. We choose it to be invariant under SU(2) × U(1) so the covariant derivative is the same as earlier 2.42.

$$\partial_\mu \Rightarrow D_\mu = \partial_\mu + igW_\mu + i\frac{g'}{2}B_\mu. \tag{2.61}$$

If we now wish to take a local gauge transformation, we must expand the state around the minimum.

$$\Phi = \frac{1}{\sqrt{2}}\begin{pmatrix} \chi_1 + i\chi_2 \\ v + h(x) + i\chi_3 \end{pmatrix}, \tag{2.62}$$

This corresponds to a physical particle appearing in our theory. As the perturbations are small, we can write this also by multiplying Φ with an exponential, which is responsible for the Goldstone bosons.

$$\Phi = e^{i\tau^i\theta^i(x)}\frac{1}{\sqrt{2}}\begin{pmatrix} 0 \\ v + h(x) \end{pmatrix}, \tag{2.63}$$

Now, although the ground state is not symmetric, the Lagrangian still must be, as we stated earlier. Therefore, by demanding SU(2) invariance, the phase can be rotated away

$$\Phi = \frac{1}{\sqrt{2}}\begin{pmatrix} 0 \\ v + h(x) \end{pmatrix}, \tag{2.64}$$

We'll drop the explicit dependence of the field h on the space time coordinate and use the gauge principle as before. By using the covariant derivative, we wish to examine the first term of the Lagrangian: $|D_\mu\phi|^2$, as it holds all the interesting kinematic contributions of the system. By inserting the covariant derivate to the term

$$D^\mu\Phi = \begin{pmatrix} \partial_\mu + i/2(gW_\mu^3 + g'B_\mu) & ig/2(W_\mu^1 - iW_\mu^2) \\ ig/2(W_\mu^1 + iW_\mu^2) & \partial_\mu - i/2(gW_\mu^3 - g'B_\mu) \end{pmatrix} \begin{pmatrix} 0 \\ v/\sqrt{2} + h/\sqrt{2} \end{pmatrix} \quad (2.65)$$

the kinetic term becomes

$$\Rightarrow |D^\mu\Phi|^2 = \frac{1}{2}(v+h)^2(0\ 1) \begin{pmatrix} \partial_\mu + i/2(gW_\mu^3 + g'B_\mu) & ig/2(W_\mu^1 - iW_\mu^2) \\ ig/2(W_\mu^1 + iW_\mu^2) & \partial_\mu - i/2(gW_\mu^3 - g'B_\mu) \end{pmatrix}^2 \begin{pmatrix} 0 \\ 1 \end{pmatrix} \quad (2.66)$$

Now the superpositions $(W_\mu^1 \mp iW_\mu^2)$, are denoted as the charged currents

$$W_\mu^\pm = \frac{(W_\mu^1 \mp iW_\mu^2)}{\sqrt{2}}. \quad (2.67)$$

There are also two other fields that correspond to the neutral currents of the weak interaction. The physical boson is denoted as

$$Z_\mu = \frac{gW_\mu^3 - g'B_\mu}{\sqrt{g^2 + g'^2}} \quad (2.68)$$

We can also form the photon with an orthogonal linear combination

$$A_\mu = \frac{gW_\mu^3 + g'B_\mu}{\sqrt{g^2 + g'^2}}. \quad (2.69)$$

The kinetic term can be then written as

$$|D^\mu\Phi|^2 = \frac{1}{2}(v+h)^2(0\ 1) \begin{pmatrix} \partial_\mu - \frac{i\sqrt{g^2+g'^2}}{2}A & -\frac{ig}{2}W^+ \\ -\frac{ig}{2}W^- & \partial_\mu + \frac{i\sqrt{g^2+g'^2}}{2}Z \end{pmatrix} \begin{pmatrix} \partial_\mu + \frac{i\sqrt{g^2+g'^2}}{2}A & \frac{ig}{2}W^+ \\ \frac{ig}{2}W^- & \partial_\mu - \frac{i\sqrt{g^2+g'^2}}{2}Z \end{pmatrix} \begin{pmatrix} 0 \\ 1 \end{pmatrix} \quad (2.70)$$

This equals to

$$|D^\mu \Phi|^2 = \frac{1}{2}\partial_\mu h \partial^\mu h + \frac{1}{2}(v+h)^2(\frac{g^2}{4}W^+W^- + \frac{1}{4}(g^2+g'^2)Z^2). \tag{2.71}$$

In this form the mass terms are visible. The bosons have acquired masses through the SSB, which equal to

$$m_W = \frac{vg}{2} \tag{2.72}$$

$$m_Z = \frac{v\sqrt{g^2+g'^2}}{2} \tag{2.73}$$

Because the photon field doesn't appear in this mass term means that the photons stay massless after the SSB as they should.

The ratio of the massive gauge bosons

$$\frac{m_W}{m_Z} = \cos\theta_W, \tag{2.74}$$

where θ is the Weinberg angle, is a phenomenologically interesting factor. It states that by measuring the Weinberg angle and the masses, the relation is a great consistency check of the SM. Indeed, the factor

$$\rho = \frac{m_W}{m_Z \cos\theta_W} \tag{2.75}$$

has been experimentally been measured to be really close to one [4].

We can write the full scalar Lagrangian 2.54, by adding the derived expression to the potential. By doing this we can find the couplings between the Higgs boson and the massive gauge bosons

$$\begin{aligned}\mathcal{L}_{scalar} = & \frac{1}{2}\partial_\mu h \partial^\mu h \\ & + \frac{m_W^2}{2}W^+W^- + \frac{m_Z^2}{2}Z^2 + \frac{-2\mu^2}{2}h^2 \\ & + \frac{m_W^2 W^+W^-}{v}h + \frac{m_W^2}{2}\frac{W^+W^-}{v^2}h^2 \\ & + \frac{m_Z^2 Z^2}{v}h + \frac{m_Z^2}{2}\frac{Z^2}{v^2}h^2 \\ & + \mu^2 v h^3 - \frac{\mu^2}{4v^2}h^4\end{aligned} \tag{2.76}$$

In this form the mass of the Higgs boson is also visible,

$$m_h = \sqrt{-2\mu^2}.$$

We stated earlier that this method has broken the $SU(2) \times U(1)$ invariance of the vacuum state. Lets examine what kind of $SU(2) \times U(1)$ transformation keeps the vacuum state invariant. This means that after the transformation

$$e^{iw^a\tau^a}e^{i\frac{\alpha}{2}}\begin{pmatrix}0\\v\end{pmatrix} = \begin{pmatrix}0\\v\end{pmatrix} \tag{2.77}$$

where we use simple notation for the VEV.

If $w^1 = w^2 = 0$ and $w^3 = \alpha$, we can see that the vacuum stays invariant.

$$e^{i\alpha\tau^3}e^{i\frac{\alpha}{2}}\begin{pmatrix}0\\v\end{pmatrix} = \begin{pmatrix}0\\v\end{pmatrix} \tag{2.78}$$

$$\rightarrow e^{i\alpha(\tau^3+Y)}\begin{pmatrix}0\\v\end{pmatrix} = \begin{pmatrix}0\\v\end{pmatrix} \tag{2.79}$$

So we can see that the $SU(2) \times U(1)$ breaks the invariance and we are left with only U(1) transformation. This is the manifestation of the SSB. We can also point out the charge of electromagnetism to really be $Q = \tau^3 + Y$ as we saw earlier! Also as we saw, the photon stayed massless after the SSB. This is because the vacuum still transforms under U(1).

We have now shown that the Higgs doublet gives masses to the gauge bosons W and Z after the SSB which supports the experimental findings. But the mass of fermions is still unexplained.

The full point of our Lagrangians is that we must add all the terms that are gauge invariant to it. We could, in fact, add a term that describes the mass of fermions to our theory. But one can't do this without trouble. If we try to form mass terms for left- and right-handed fermions we get objects that are of the form

$$\Delta\mathcal{L} = -M(\psi_L^\dagger \psi_R + \psi_R^\dagger \psi_L) \tag{2.80}$$

These terms are not gauge invariant. This can be seen by examining an object of a form

$$-m_e e_L^\dagger e_R. \tag{2.81}$$

The term is not gauge invariant as the left-handed object transforms under SU(2) but the right-handed object doesn't. The fields also have different U(1) charges, meaning that the hypercharge is not conserved.

This problem can be tackled by introducing Yukawa couplings. We can write a gauge invariant object like

$$\Delta\mathcal{L} = -y_e \bar{E}_L H e_R, \tag{2.82}$$

where we can use the Higgs doublet H to connect the SU(2) indices. As the both fermion fields carry Lorentz indices but the scalar field does not, we can state that the term is indeed also Lorentz invariant. The term also doesn't violate the conservation of the hypercharge as the sum of the hypercharges sum to zero:

$$\Delta Y = \frac{1}{2} + \frac{1}{2} - 1 = 0 \tag{2.83}$$

Now after the symmetry breaking, the Higgs doublet develops a VEV. At low order, we can replace the field with the VEV, so the mass term becomes

$$\Delta\mathcal{L} = -\frac{y_e}{\sqrt{2}} \nu e_L^\dagger e_R, \tag{2.84}$$

where we can see that the electron has a mass proportional to the Yukawa coupling and the Higgs VEV.

Similar kind of procedure can be done to other fermions as well and one can see that as we don't have right-handed neutrinos in the SM, we can't generate mass for neutrinos within the SM. This is also somewhat a problem as neutrino oscillation suggest that neutrinos have a small mass [28] but we'll cover this later in this chapter.

For every fermion the Yukawa coupling y is different and it is proportional to the mass of the fermion divided by the VEV. We have now generated masses for the SM particles through the SSB and Yukawa couplings.

The spontaneous symmetry breaking and the Yukawa coupling could be verified by observing the Higgs boson. At the European Organization for Nuclear Research (CERN), in the Large Hadron Collider (LHC), located in Geneva, researchers observed this boson in 2012. The observation was done by CMS and ATLAS collaborations. This was maybe one of the most exiting findings of particle physics [12] [8]. Now all the particles in the Standard Model have been detected and we have not yet observed any particles that wouldn't be described by the the SM.

2.6 Radiative corrections

When using quantum field theory, we use Feynman rules to calculate two point functions, or correlators between two or multiple points in space-time. From them, we can calculate amplitudes and finally physical observables, such as cross sections. When calculating the amplitude of a processes in QFT, we face problems with converging integrals. To move on with these problems we must add so called counterterms to cancel the infinities. By adding these counterterms to propagators and vertices of our Feynman graphs we also get finite contributions that make the values of our calculations more precise. This might sound non-intuitive, but we can measure for example the coupling constant of QED. If we compare the measurement to our calculation we notice that indeed we must add these counterterms to get the accurate result.

When we calculate for example cross sections using Feynman graphs that don't have loops in them, we say that we are considering processes at the tree-level. All these processes also receive higher order contributions called radiative corrections from the diagrams that have loops. The emission of extra photon in the initial or final state, called bremsstrahlung, is also a radiative correction. In addition to these physical loop-integrals we have so called Faddeev-Popov ghost fields. These fields are anticommutating scalar fields that we need in order to calculate counter terms in non-abelian gauge theories [26].

By adding these loop-integrals to Feynman graphs of our interaction, we get more precise values for different physical observables. In theory, we should add all the possible Feynman graphs together to get the most accurate result, but in practice this is not possible as there are infinite number of loop diagrams. Depending on the size of the coupling constant of the theory, the major contribution to the observable comes from the few first diagrams. Depending on are we calculating a correction to the propagator, to a vertex or even to a full interaction of multiple particles, we get corrections to different observables. If we for example want to find the corrections

to the Higgs boson mass.

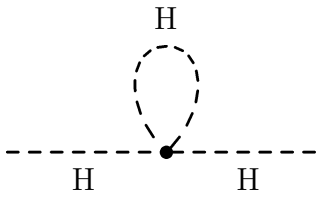

Figure 2.4: The loop contribution to Higgs bosons mass with a Higgs boson loop

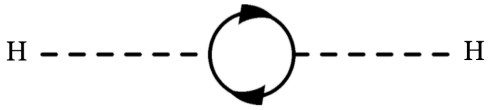

Figure 2.5: The loop contribution to Higgs bosons mass with a fermion loop

At loop level, there are two corrections to the Higgs field self-energy, or more familiarly its mass. These loop diagrams are presented in Figures 2.4 and 2.5. If we calculate the mass of the Higgs boson, we must sum all the terms together. With the corrections, the mass becomes, with loop momentum being k:

$$m_h\phi^\dagger\phi = \sqrt{2}\mu\phi^\dagger\phi + \int^\Lambda + \lambda\frac{d^4k}{k^2 - 2mu^2} + g^2\int^\Lambda + \lambda\frac{d^4k}{\not{k}\not{k}} \tag{2.85}$$

$$\sim \sqrt{2}\mu\phi^\dagger\phi + \lambda\Lambda^2\phi^\dagger\phi - g^2\Lambda^2\phi^\dagger\phi \tag{2.86}$$

$$= (\sqrt{2}\mu + (\lambda - g^2)\Lambda^2)\phi^\dagger\phi, \tag{2.87}$$

where we used cut-off regularization. From this, we can state that the mass goes as the square of the Planck scale Λ. It is defined as the scale where one can't forget the effects of gravity, $\lambda = 10^{19}$GeV and is used as the threshold of the SM. Since SM doesn't predict Higgs bosons mass, we are able to set μ to compensate the correction, so that the mass becomes the observed 125 GeV/c^2. This is so called fine tuning problem; how can we, and why should we, fine tune the factor μ to be so

low if the correction is of the order of 10^{28} GeV/c^2. This is one of the unanswered questions of the SM.

2.7 Open questions in the Standard Model

As discussed earlier, the SM doesn't seem to be complete. The radiative corrections lead to the fine tuning problem. This is not the only problem we face when using the SM. The number of free parameters in the SM is not well understood. There are in total 19 of them: coupling strengths of gauge bosons and masses of quarks and leptons to mention a few. Also SM doesn't explain neutrino masses which we know to exist as neutrinos must have a small mass because of the neutrino oscillation [28].

The SM also lacks a candidate for cold dark matter which is essential to describe multiple phenomena from the surrounding universe. Dark matter is needed to describe for example the formation of galaxies [42] and we would need a very weakly interacting particle to explain dark matter. SM doesn't say anything about gravity as well. We don't understand why the scale of gravity is so much larger than the scale of weak interaction which is not natural as one would expect all the factors to be of the same order. The baryon asymmetry is a problem as well. SM doesn't tell us why there seems to be more matter than antimatter. The CP violation could be one of the answers to this asymmetry, but there are problems with the CP violation as well.

There is a problem with the CP and strong interaction. In QCD, one could add an additional term to the Lagrangian, which would be allowed by the gauge invariance. This term would also be a source of CP violation in the theory. Although approved by the gauge invariance, this term would predict an electric dipole moment for neutrons which is much larger than the measured one. Solution to this problem could be described with models introducing hypothetical particles called axions [23].

Multiple theories try to solve these problems for example multidimensional models and string theory but in this work we will focus on one. We will discuss in the Chapter 4, a beyond the standard model theory called supersymmetry. If we add a minimal substitution from it to the SM, we can tackle some of these open questions. Supersymmetry has not been observed at low energies but as the theory requires additional scalar doublets, one could find indications of supersymmetry if these additional scalar bosons were discovered. Therefore we'll discuss the two-Higgs-doublet-models in greater detail first, as they predict additional Higgs particles that play a major role in the data analysis part of this thesis.

3. The two-Higgs-doublet-models

In this chapter we'll discuss the two-Higgs-doublet-models (2HDM). Compared to the SM, an additional scalar doublet is introduced to the theory. This addition is motivated by multiple solutions to the problems of the SM. It leads to new physical particles and also predicts new phenomena, such as additional sources of CP violation [35]. We'll see that the 2HDM results in multiple new Higgs bosons after the spontaneous symmetry breaking (SSB). In the second section, we'll discuss the production and decay modes of some of these particles.

3.1 Spontaneous symmetry breaking in the 2HDM

When considering beyond the SM theories, a parameter defined using the W and the Z boson masses and the gauge couplings becomes important. The ratio ρ has experimentally been observed to be really close to one. In terms of weak isospin, hypercharge and the vacuum expectation value, at tree level, it becomes

$$\rho = \frac{m_W^2}{m_Z^2 \cos^2 \theta_W} = \frac{\sum_{i=1}^{n} (4\tau_i(\tau_i + 1) - Y_i^2) \frac{|v_i|^2}{2}}{\sum_{i=1}^{n} 2Y_i^2 |v_i|^2}. \tag{3.1}$$

This value must agree with the experimental results and must be close to one. If we add additional Higgs SU(2) doublet, it constrains the doublet to have a hyperchage $Y^2 = 1$.

We now introduce two scalar doublets, with both having Y = 1

$$\Phi_1 = \begin{pmatrix} \phi_1^+ \\ \phi_1^0 \end{pmatrix}, \Phi_2 = \begin{pmatrix} \phi_2^+ \\ \phi_2^0 \end{pmatrix} \tag{3.2}$$

This gives in total eight degrees of freedom. With two Higgs doublets the potential term of the Lagrangian becomes [35]:

$$V_H = m_{11}^2 \Phi_1^\dagger \Phi_1 + m_{22}^2 \Phi_2^\dagger \Phi_2 - (m_{12}^2 \Phi_1^\dagger \Phi_2 + h.c.) \tag{3.3}$$

$$+ \frac{\lambda_1}{2}(\Phi_1^\dagger \Phi_1)^2 + \frac{\lambda_2}{2}(\Phi_2^\dagger \Phi_2)^2 + \lambda_3(\Phi_1^\dagger \Phi_1)(\Phi_2^\dagger \Phi_2) \tag{3.4}$$

$$+ \lambda_4(\Phi_1^\dagger \Phi_2)(\Phi_2^\dagger \Phi_1) + \frac{\lambda_5}{2}((\Phi_1^\dagger \Phi_2)^2 + h.c.) \tag{3.5}$$

$$+ \lambda_6(\Phi_1^\dagger \Phi_1)(\Phi_1^\dagger \Phi_2) + \lambda_7(\Phi_2^\dagger \Phi_2)(\Phi_1^\dagger \Phi_2) + h.c. \tag{3.6}$$

where *h.c.* stands for hermitian conjugate. The next step of the SSB would be to minimize this potential with respect to the different fields, and expand the field in the minimum like we did in the case of the SM. First, we need to hold constraints, so that we can minimize the potential.

In the SM there appears flavour changing neutral currents (FCNC) only at loop level. The FCNC is an interaction, where the flavour of a quark is changed by a Z boson. The changing of a flavour means for example that a strange quark changes to a down quark. To have no FCNC in the theory one must choose $m_{12} = \lambda_6 = \lambda_7 = 0$.

We can hold other constraints as well. We must make sure the vacuum is stable. This means that there is no such direction that makes the potential $V_H = -\infty$. In other words we make sure, that we really expand the potential in a stable minimum. This gives constraints to the quadratic couplings. In the case $\lambda_6 = \lambda_7 = 0$, the vacuum stability constraint gives [30]:

$$\lambda_1 > 0, \lambda_2 > 0, \lambda_3 + \sqrt{\lambda_1 \lambda_2} > 0, \lambda_3 + \lambda_4 - |\lambda_5| + \sqrt{\lambda_1 \lambda_2} > 0 \tag{3.7}$$

In the 2HDM the minimum of the potential can be found, similarly to SM case

$$\frac{\partial V}{\partial \Phi_i^\dagger} = 0 \tag{3.8}$$

In a general case, the minimum gets a form

$$\Phi_1 = \frac{1}{\sqrt{2}} \begin{pmatrix} 0 \\ v_1 \end{pmatrix} \tag{3.9}$$

$$\Phi_2 = \frac{1}{\sqrt{2}} \begin{pmatrix} w \\ v_2 e^{i\xi} \end{pmatrix} \tag{3.10}$$

Now the phase appearing in the second VEV is a source of a CP violation. We can allow CP violation by setting $\xi \neq 0$. If we don't allow CP violation we set $\xi = 0$.

Also, by choosing $w \neq 0$, we could describe charged vacuum. In such case the U(1) symmetry gets broken and charge is not conserved. Choosing $w = 0$ gives a neutral vacuum.

These VEVs lead to a phenomenologically interesting parameter with parametrization $v_1 = v\cos\beta$ and $v_2 = v\sin\beta$

$$\tan\beta \equiv \frac{v_2}{v_1}. \tag{3.11}$$

In order to have a model with same masses for Z and W bosons as in the SM, we must demand

$$v_1^2 + v_2^2 = v^2 \tag{3.12}$$

with $v^2 = \frac{1}{\sqrt{2}\mathrm{G}_F} \sim 246^2\mathrm{GeV}^2$, G_F being the Fermi constant.

Now to demonstrate SBB in the 2HDM, we assume CP conservation, small sources of FCNC at tree level and neutral vacuum. In other words, we choose $\lambda_6 = \lambda_7 = 0$ and $\xi = w = 0$. Small sources of FCNC can be allowed by setting m_{12} real. Then we take a derivative of the potential with respect to the fields.

$$\frac{\partial V}{\partial \Phi_i^\dagger}|_{\Phi_i = v_i/\sqrt{2}} = 0 \tag{3.13}$$

which gives

$$m_{11}^2 = m_{12}^2\tan\beta - \frac{v^2}{2}(\lambda_1\cos^2\beta + (\lambda_3+\lambda_4+\lambda_5)\sin^2\beta) \tag{3.14}$$

$$m_{22}^2 = m_{12}^2\tan^{-1}\beta - \frac{v^2}{2}(\lambda_2\sin^2\beta + (\lambda_3+\lambda_4+\lambda_5)\cos^2\beta) \tag{3.15}$$

Then we must expand the the field in the minimum. In case of two scalar doublets, the expanding gives eight fields

$$\Phi_i = \begin{pmatrix} \phi_i^+ \\ \frac{1}{\sqrt{2}}(v_i + \rho_i + i\eta_i) \end{pmatrix}, i = 1,2 \tag{3.16}$$

With this, we can find the mass terms from the potential. There appears a mass

term for the charged scalars, where $\phi_i^{+*} = \phi_i^-$.

$$\mathcal{L}_{m_{\phi^\pm}} = (m_{12}^2 - (\lambda_4 + \lambda_5)v_1v_2)(\phi_1^- \ \phi_2^-) \begin{pmatrix} \frac{v_2}{v_1} & -1 \\ -1 & \frac{v_1}{v_2} \end{pmatrix} \begin{pmatrix} \phi_1^+ \\ \phi_2^+ \end{pmatrix} \tag{3.17}$$

To find the mass of the physical particles we must diagonalize the matrix in the mass term. With

$$(\frac{m_{12}^2}{v_1v_2} - (\lambda_4+\lambda_5)) \begin{pmatrix} v_2^2 & -v_1v_2 \\ -v_1v_2 & v_1^2 \end{pmatrix} = (\frac{m_{12}^2}{v_1v_2} - (\lambda_4+\lambda_5)) \begin{pmatrix} \frac{v_1}{v} & -\frac{v_2}{v} \\ \frac{v_2}{v} & \frac{v_1}{v} \end{pmatrix} \begin{pmatrix} 0 & 0 \\ 0 & v^2 \end{pmatrix} \begin{pmatrix} \frac{v_1}{v} & \frac{v_2}{v} \\ -\frac{v_2}{v} & \frac{v_1}{v} \end{pmatrix} \tag{3.18}$$

Now by diagonalizing the matrix we've moved to a mass-basis. In the mass-basis the diagonal entries describe the physical masses. The charged Higgs bosons are denoted as $H^\pm$ and there also appears two charged Goldstone bosons. The physical states for the charged Higgs bosons and the Goldstone bosons are then defined as

$$\begin{pmatrix} G^\pm \\ H^\pm \end{pmatrix} = \begin{pmatrix} \cos\beta & \sin\beta \\ -\sin\beta & \cos\beta \end{pmatrix} \begin{pmatrix} \phi_1^\pm \\ \phi_2^\pm \end{pmatrix} \tag{3.19}$$

One can then see that the mass term for the charged Higgs boson, in the mass-basis, is

$$\mathcal{L}_{m_{\phi^\pm}} = v^2(m_{12}^2 - (\lambda_4 + \lambda_5)v_1v_2)(G^- \ H^-) \begin{pmatrix} 0 & 0 \\ 0 & 1 \end{pmatrix} \begin{pmatrix} G^+ \\ H^+ \end{pmatrix} \tag{3.20}$$

The term clearly states that the charged Goldstone bosons are massless. The second diagonal element describes the mass of the charged Higgs bosons. The masses are then

$$m_{H^\pm}^2 = (\frac{m_{12}^2}{v_1v_2} - (\lambda_4 + \lambda_5))(v_1^2 + v_2^2) \tag{3.21}$$

The mass term for the pseudoscalar can then be found similarly by considering

$$\mathcal{L}_{m_\eta} = (\frac{m_{12}^2}{v_1v_2} - 2\lambda_5)(\eta_1 \ \eta_2) \begin{pmatrix} v_2^2 & -v_1v_2 \\ -v_1v_2 & v_1^2 \end{pmatrix} \begin{pmatrix} \eta_1 \\ \eta_2 \end{pmatrix} \tag{3.22}$$

After the diagonalization, the mass for the pseudoscalar, denoted by A^0 becomes

$$m_A^2 = (\frac{m_{12}^2}{v_1 v_2} - 2\lambda_5)(v_1^2 + v_2^2) \tag{3.23}$$

And again, the Goldstone boson remains massless.

The CP-even scalars can be found by considering

$$\mathcal{L}_{m_\rho} = -(\rho_1 \ \rho_2) \begin{pmatrix} m_{12}^2 \frac{v_2}{v_1} + \lambda_1 v_1^2 & -m_{12}^2 + (\lambda_3 + \lambda_4 + \lambda_5) v_1 v_2 \\ -m_{12}^2 + (\lambda_3 + \lambda_4 + \lambda_5) v_1 v_2 & m_{12}^2 \frac{v_1}{v_2} + \lambda_2 v_2^2 \end{pmatrix} \begin{pmatrix} \rho_1 \\ \rho_2 \end{pmatrix} \tag{3.24}$$

The rotation angle α performs the diagonalization of this matrix. By diagonalizing this matrix one finds that the Goldstone boson doesn't disappear. There appears two additional Higgs bosons from this term, denoted with h^0 and H^0.

So if we denote

$$(M_\rho^2)_{ij} = M_{ij} = \begin{pmatrix} m_{12}^2 \frac{v_2}{v_1} + \lambda_1 v_1^2 & -m_{12}^2 + (\lambda_3 + \lambda_4 + \lambda_5) v_1 v_2 \\ -m_{12}^2 + (\lambda_3 + \lambda_4 + \lambda_5) v_1 v_2 & m_{12}^2 \frac{v_1}{v_2} + \lambda_2 v_2^2 \end{pmatrix}, \tag{3.25}$$

where the i, j are the matrix elements, one finds the mass for the CP-even scalars of

$$m_{H^0,h^0} = M_{11} + M_{22} \pm \sqrt{(M_{11} - M_{22})^2 + 4M_{12}^2}, \tag{3.26}$$

making the other Higgs boson H^0 heavier than h^0.

After the SBB the eight degrees of freedom have changed to five physical Higgs bosons: one neutral, CP-even light h and heavier H. One neutral, CP-odd A and two charged Higgs bosons $H^\pm$. One can then find the couplings between the SM gauge bosons and the five Higgs bosons by moving to so called Higgs basis

$$\Phi_{HB} = -\sin\beta \Phi_1 + \cos\beta \Phi_2$$

and by considering the kinetic term

$$D^\mu \Phi_{HB}^\dagger D_\mu \Phi_{HB}$$

with the same covariant derivatives as in the SM case.

There appear different types of 2HDM, which differ in the way how the scalar doublets couple to quarks and leptons. In this thesis we'll focus on the type II 2HDM, where the right handed quarks, with charge $q = -1/3$, together with leptons, couple to one doublet and the right handed quarks, with charge $q = 2/3$, couple to the other. In other words, the down type quarks and leptons, by convention, couple to the Φ_1 doublet and the up-type quarks couple to the Φ_2 doublet. Type II 2HDM is maybe the most interesting as it presents minimal supersymmetric Standard Model (MSSM) as a special case.

The fermion masses are generated through the Yukawa coupling in the 2HDM, similarly to the SM case. The only difference is that if we want to generate the same masses to the fermions as in the SM, we need to take into account the α and β factors in the Yukawa couplings. The factor α is the rotation angle of the CP-even scalars and β is the factor appearing in the ratio of the VEVs.

3.2 The production and decay of the charged Higgs boson

The production and decay of the $H^{\pm}$ depends on the mass of the charged Higgs bosons. If the charged Higgs boson mass is larger than the difference between a top and a bottom quark $m_{H^{\pm}} > m_t - m_b$, we call the charged Higgs boson heavy. In that case, it is produced through $\bar{t}b \to H^+$ as in Figure 3.1 for four-flavour scheme and in Figure 3.2 for five-flavour scheme. These schemes represent the way how we perturbatively order the terms in the calculations. The results are identical if one takes all terms into account, but at finite order 4FS and 5FS give different results. The full cross section can be then calculated by using the "Santander matching scheme" by combining the four- and five-flavour results [33].

If the charged Higgs boson mass is smaller than the difference between a top and a b-quark $m_{H^+} < m_t - m_b$, we say that the Higgs boson is light. Then the light charged Higgs boson is produced through $t \to H^+b$ as illustrated in Figure 3.3.

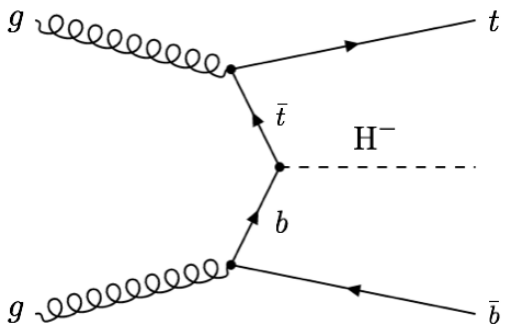

Figure 3.1: Production of the heavy charged Higgs boson in the four-flavour scheme.

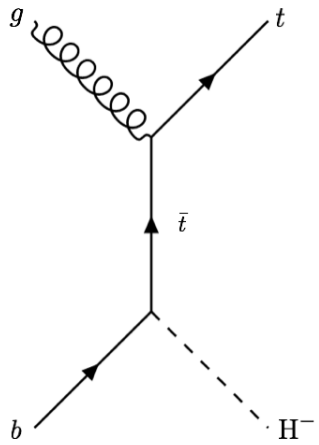

Figure 3.2: Production of the heavy charged Higgs boson in five-flavour scheme

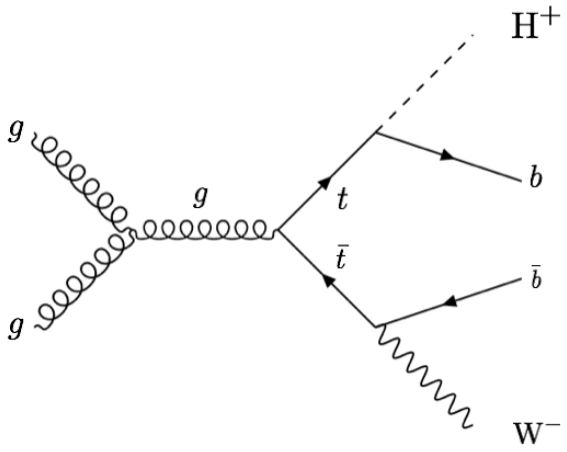

Figure 3.3: Production of the light charged Higgs boson

The decay of the charged Higgs boson is also affected by the mass of the boson. If the charged Higgs boson is heavy ($m_{H^+} > m_t - m_b$), the decay modes $H^+ \to \tau^+\nu_\tau$ and

$H^+ \to t\bar{b}$ are dominant. The branching ratio for different final states are illustrated in Figure 3.4.

If the charged Higgs boson is light ($m_{H^+} < m_t - m_b$), the $H^+ \to \tau^+\nu_\tau$ is the dominant decay mode. The decay to the final state with hadronic τ lepton is illustrated in Figure 3.5 for the light charged Higgs boson and in the Figure 3.6 for the heavy charged Higgs boson respectively.

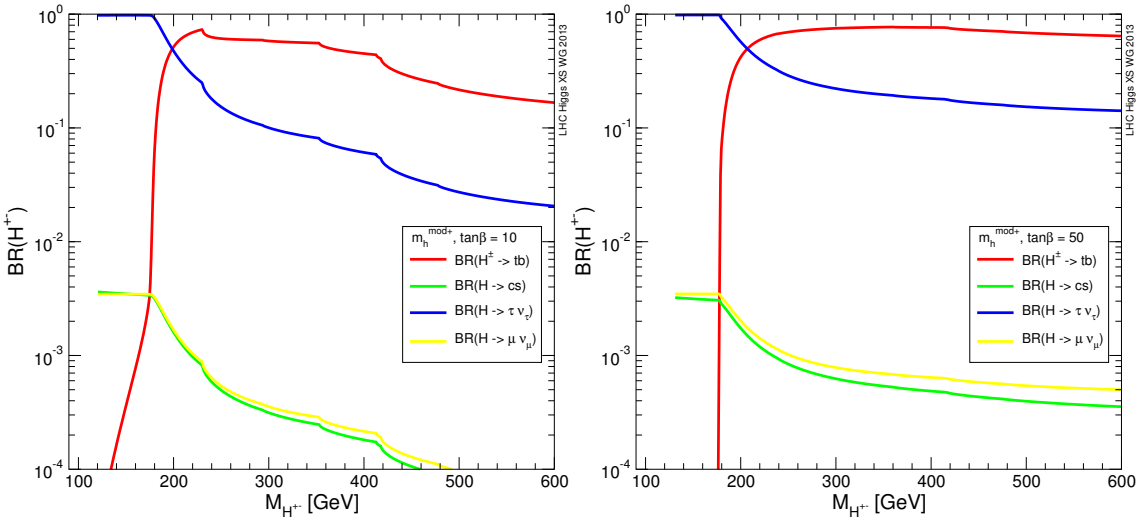

Figure 3.4: Branghing ratios of the charged Higgs boson to different final states. Left for $\tan\beta = 10$ and right for $\tan\beta = 50$ [1].

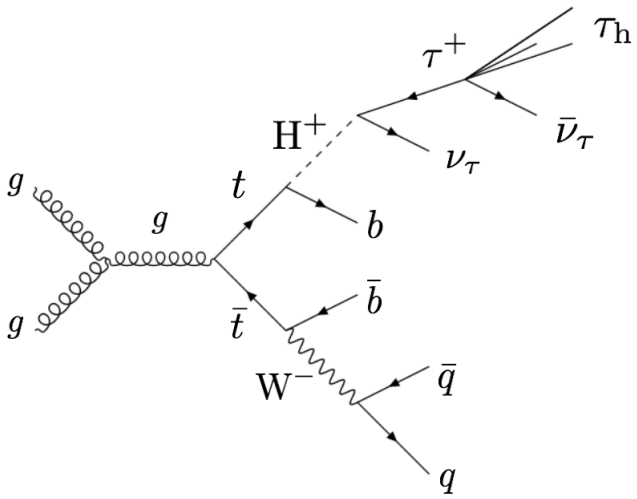

Figure 3.5: Decay of the light charged Higgs boson through $\tau\nu$ to a final state with a hadronic τ lepton.

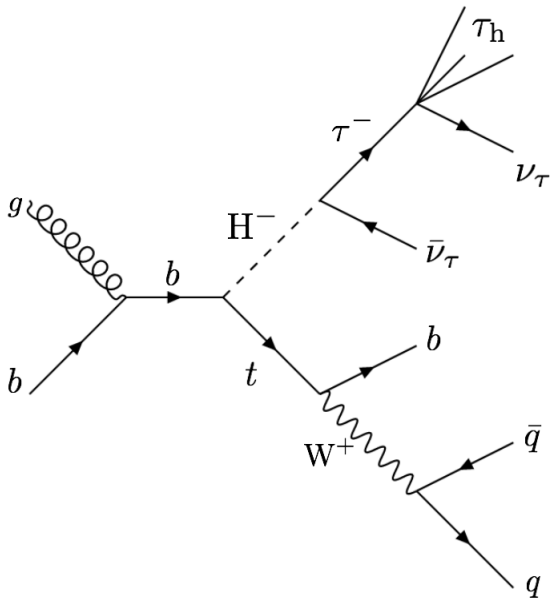

Figure 3.6: Decay of the heavy charged Higgs boson through $\tau\nu$ to a final state with a hadronic τ lepton.

Final states with cs and $\mu\nu$ are possible, but they have smaller branching ratio. It is also good to keep in mind that the value of $\tan\beta$ is a free parameter when considering the production and decay of the charged Higgs boson.

There is also the intermediate mass range for the charged Higgs boson, where the mass of the charged Higgs boson is close to the top quark mass. In that case both earlier production mechanisms contribute and the effect of finite top-width and the interference of resonant and non-resonant diagrams must be taken into account. Theoretical calculations considering the cross section have been performed with a complex-mass scheme in the 4FS to next-to-leading order [22].

3.3 Supersymmetry and the minimal supersymmetric Standard Model

Supersymmetry (SUSY) gives rise to multiple new particles. In SUSY, every particle gets its superpartner. The superpartner of a boson is a fermion, and a superpartner of a fermion is a boson. This way, the particles and their superpartners differ in spin by a half-integer. As we have not detected these superpartners, the symmetry responsible for the link between bosons and fermions must be broken [27]. Therefore the superpartners could have much larger mass than the particles we observe.

The minimal supersymmetric Standard Model (MSSM) takes the minimal number

of new particles and interactions from SUSY to the SM. It also requires two Higgs SU(2) doublets, and is a type II 2HDM. This allows multiple problems of the SM to be solved. For example, the fine tuning problem, appearing in the intermediate loops in the correction of the SM Higgs boson mass, gets solved with MSSM. The MSSM predicts a superpartner of the top quark, a stop quark. The contribution of the stop quark would have to be included to the radiative corrections. This loop, mediated by the stop quark, would equally cancel the term responsible of the fine tuning problem [36]!

Also, MSSM predicts a heavy superpartner of gauge bosons, called neutralino. These really weakly interacting particles are considered as a good candidate for dark matter as the lightest neutralino would be stable, weakly interacting and massive. Also as we saw there is a possibility to generate additional sources of CP-violation in the extended Higgs sector.

Although the MSSM offers quite many solutions it doesn't answer all of them. By introducing the new superfields to our theory, the number of free parameters rises drastically. Also, the rise of additional sources of CP-violation, rises the question, why do we experimentally see so small amount of CP-violation in nature?

4. The CMS experiment

We'll discuss the experimental setup of the CMS experiment at CERN, which led to the discovery of the Higgs boson together with the ATLAS experiment.

4.1 The Large Hadron Collider

The Large Hadron Collider (LHC) is at the moment the worlds largest particle accelerator, with a circumference of 27 km. The long circumference makes high energies possible and the LHC is designed to collide proton beams with an energy of $\sqrt{s} = 14$ TeV and at an instantaneous luminosity of 10^{34} cm$^{-2}s^{-1}$ [25].

The proton beams can be accelerated by using electric fields. Before entering the LHC, the protons are accelerated by using multiple smaller accelerators. The proton beams can be kept on the round track with magnets while other magnets take care that the proton bunches in the beams don't fall apart. The beams travel in two adjacent beam pipes to opposite directions from where the beams can be guided to collision points. The detectors are located in these places where the beams are allowed to collide.

There are in total four different collision points and seven experiments at the LHC. The experiments are ATLAS, CMS, ALICE, LHC-b, LHC-f, TOTEM and MoEDAL. ATLAS and CMS are called general-purpose detectors as they are used to detect many phenomena of physics such as production of the Higgs boson. The other experiments are more specified to certain phenomena. ALICE is dedicated in the research of the quark-gluon plasma using heavy-ion collisions. The quark-gluon-plasma is the matter that dominated the early universe. Therefore, by studying it, we can form a better understanding of the phenomena that were present in the early seconds of the universe.

LHC-f, or LHC forward, is used to research cosmic ray models in laboratory conditions. Results of the LHC-f experiment can then be used to better understand high energy cosmic ray showers that hit the Earths atmosphere. LHC-b, standing for LHC beauty, investigates the interaction of b quarks. By studying hadrons contain-

ing b quarks, one can study CP violation, which is one of the main research aspects of the LHC-b.

TOTEM is used to investigate the total cross section and diffractive processes, giving the name: "total, elastic and diffractive cross-section measurement" to the experiment. Monopole and exotics detector at the LHC, or simply MoEDAL, is used to search for magnetic monopoles. This is a more passive experiment at the side of the LHC-b experiment, where the researchers try to capture a magnetic monopole to plastic plates. Few times a year the plastic plates are then put through a coil to detect if a magnetic monopole have been created at the collision and been captured between the polymer chains.

4.2 The Compact Muon Solenoid

The Compact Muon Solenoid (CMS) [11] is designed to detect muons as efficiently as possible. As many other detectors, the CMS also consists of several layers dedicated to detecting different particles. A perspective view of the CMS detector is given in Figures 4.1 and 4.2. Every layer has its own specific purpose and we'll consider each of the layers separately in the following subsections. To detect and measure the particles that form in the proton-proton collisions we also need a magnet field in the interaction point and the first three subdetectors are located inside a superconducting solenoid.

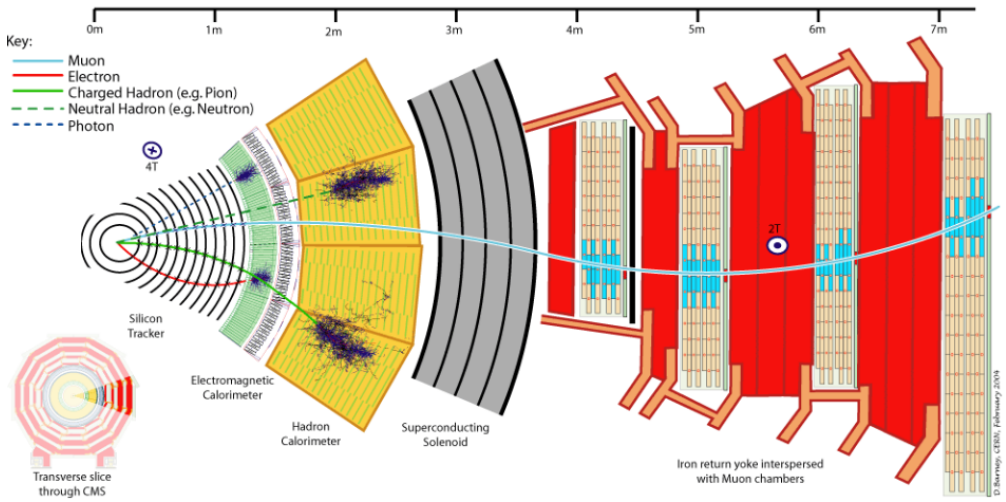

Figure 4.1: A slice of the CMS detector [21]

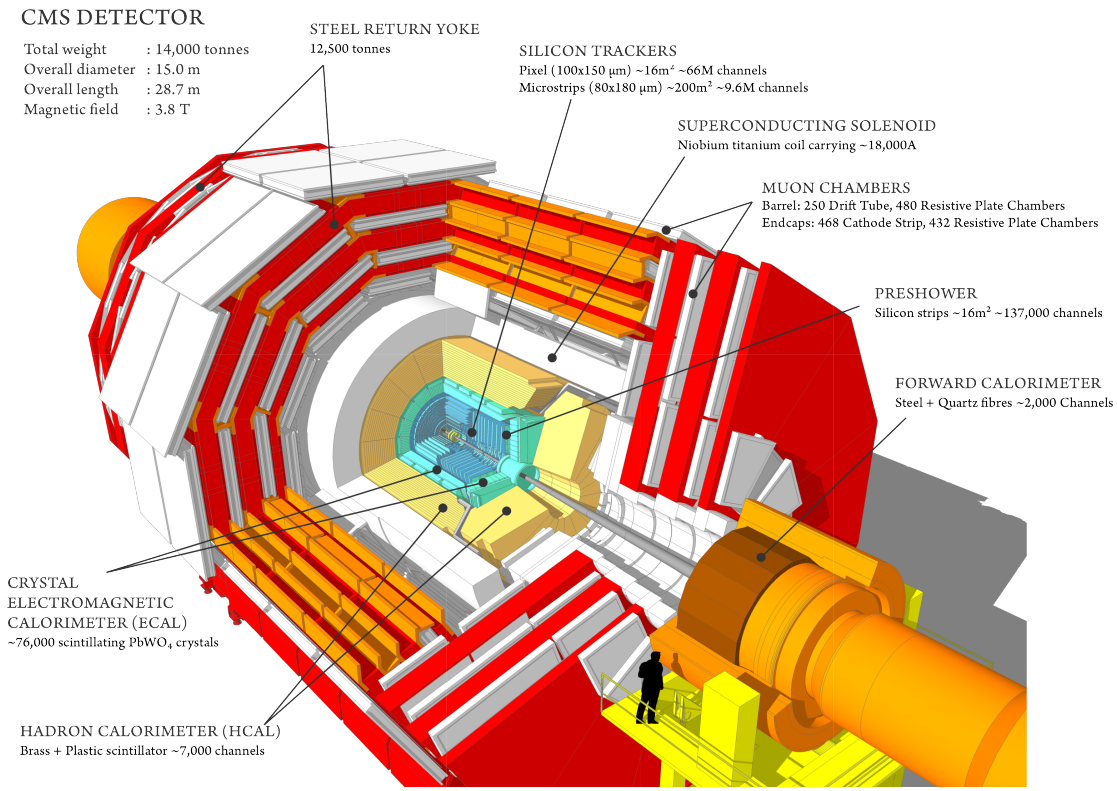

Figure 4.2: A view inside the CMS detector [41]

4.2.1 Tracking system

The tracking system of CMS is designed to give us an efficient measurement of trajectories of charged particles that form in the beam collisions. The tracker surrounds the interaction point for a length of 5.8 m and a diameter of 2.5 m. A homogeneous magnetic field of 3.8 T is created with a solenoidal magnet. The magnetic field bends the trajectories of charged particles and due to this bending one can measure the momentum and the charge of the particle. More momentum means less bending and vice versa. Positively charged particles bend to the opposite direction than negatively charged ones, so we can deduce the charge of the particle from the trajectory.

The intense particle flux causes severe radiation damage. Therefore the main challenge in the design of the tracking system was to develop components that resist radiation. Also the huge amount of particles forming in the collisions require detec-

tion technology with a fast response time.

These requirements led to the use of silicon detector technology. The CMS tracker consists of a pixel detector with three barrel layers and a silicon strip tracker with 10 barrel detection layers. The pixels are located at radius of 4.4 cm and 10.2 cm and the strips extend the tracking system all the way to 1.1 m. There are also endcap disks to provide wider range in the position measurement.

The charged particles, that hit the silicon layers, produce an electric signal through ionization processes, which is then shaped and amplified. With the amplified signals, one can reconstruct vertices inside the tracker. The tracker needs to reconstruct the primary vertices and the secondary vertices as well. The primary vertices are created right at the proton collision points and the secondary vertices are a signature of a decay of a particle. The pixel detector, being close to the interaction point, makes an accurate impact parameter measurement possible. Impact parameter is the shortest distance between the particle trajectory and the primary vertex.

4.2.2 Calorimeters

Outside the tracker there are two different calorimeters. The function of the calorimeters is to detect and measure the energy of particles. There are two different types of calorimeters: electromagnetic calorimeter (ECAL) for measuring the energy of electrons and photons and hadron calorimeter (HCAL) for measuring the enrgy of the hadrons.The energy is measured by making the particle loose its energy.

The ECAL of CMS is made of a lead tungstate ($PbWO_4$) crystals. The crystals make it possible to design a calorimeter which is fast and radiation resistant, which is important for the use in the LHC. The crystals scintillate when electrons and photons pass through them. The material is sufficient as the scintillation decay time of the crystal is of the same order with the particle beam collisions. The amount of light produced by the crystal is proportional to the energy of the passed particle. The small light yield of the crystals are then amplified with photodetectors. The ECAL extends from the tracker to the radius of 1.77m.

Photons and electrons are measured by the ECAL and with the help from the tracking system the impact parameters can be calculated. The extinction between electrons and photons can be done, as photons are not affected by the tracker.

The HCAL is the outermost part located inside the CMS solenoid with a radius of 2.95 m. As the volume is restricted by the solenoid, an outer part called a tail catcher is placed outside the solenoid. A forward hadron calorimeter is added to extend the coverage close to the beam pipe, as presented in Figure 4.2.

HCAL is made of brass and is built with alternating layers of absorber and scin-

tillator materials. The HCAL can detect the position, energy and arrival time of particles. When a particle passes through the calorimeter, the scintillation layers emit photons and the signals are measured.

4.2.3 Muon detector

The muon detectors are located outside the CMS solenoid. Muons can be used in multiple analyses as they are the signature of many interesting events over a high background rate. This means that we can detect interesting particles from a large amount of not so interesting events, by examining muons.

There are three types of subdetectors in the CMS for muon detection. When gas in the detector is ionized, the electrons and ions in the gas form a current flow, which can then be measured. In the CMS, drift tubes (DT), cathode strip chambers (CSC) and a system of resistive plate chambers (RPC) are used to detect muons.

The DT chambers are used in the barrel region where the muon rate is low. The DT chambers are made from cells filled with gas mixture of Argon and CO_2 with an anode wire in the middle and the cathode surfaces on the sides. This way the ionizing particle can form the current flow.

The CSC have faster response time, so they are located in the endcaps, where the muon and background levels are higher. The cells of CSC have multiple wires in the middle and the cathodes on the top and bottom of the cell.

The RPC's are located in the barrel and in the endcap regions. The RPC's is a double-gap chamber and readout strips are also planted in the chamber. Charged particles ionizes the gas and the avalanche is then measured by the readout strips. The RPC's are dedicated to triggering. The trigger system decides whether to save the data of an event or not.

Together with the calorimeters and the muon detector, the missing transverse energy can be measured. The missing transverse energy is used in neutrino detection. Neutrinos can't be detected directly, as they interact so weakly, so one must try to find unbalances in the momentum. The transverse momentum of the colliding protons is zero, so by measuring the transverse momentum of the particles hitting the detector, one can find the transverse energy of the missing particles.

5. The CMS trigger system

The beam crossing interval of the LHC is 25 ns. This means that proton beams collide inside the CMS 40 000 000 times per second, which makes the storing of the data a problem. This is why we need triggers: we must choose the interesting events and forget the rest due to limited write speed. With the trigger system we reduce the output rate of 1 GHz first to 100 kHZ and finally to 400 Hz to be able to save the data.

Trigger is the start of the physics event selection process, and the rate is reduced in two steps at the CMS. First is the Level-1 trigger (L1) and the second is the high-level trigger (HLT). This chapter is based on [15] and [10].

5.1 Level 1 trigger system

The Level-1 trigger is implemented in the hardware. The trigger system decides if an event is passed to the HLT or not. The information comes from the calorimeter and muon detectors. The Level-1 trigger consists of calorimeter, muon and global trigger systems. The Level-1 trigger reduces the rate of events from 1 GHz to 100 kHz.

5.1.1 Calorimeter trigger system

From the calorimeters the energy and quality of an event is passed to a regional calorimeter trigger. The data flows in 24 bits containing the information. The regional calorimeter trigger then sends electron and photon candidates and regional transverse energy sums to the second stage.

The information then comes to a global calorimeter trigger, which sorts the candidates and finds jets from the energy sums. This also allows calculation of the missing transverse energy. This information is then sent to a global trigger (GT), which is the final state of the Level-1 trigger.

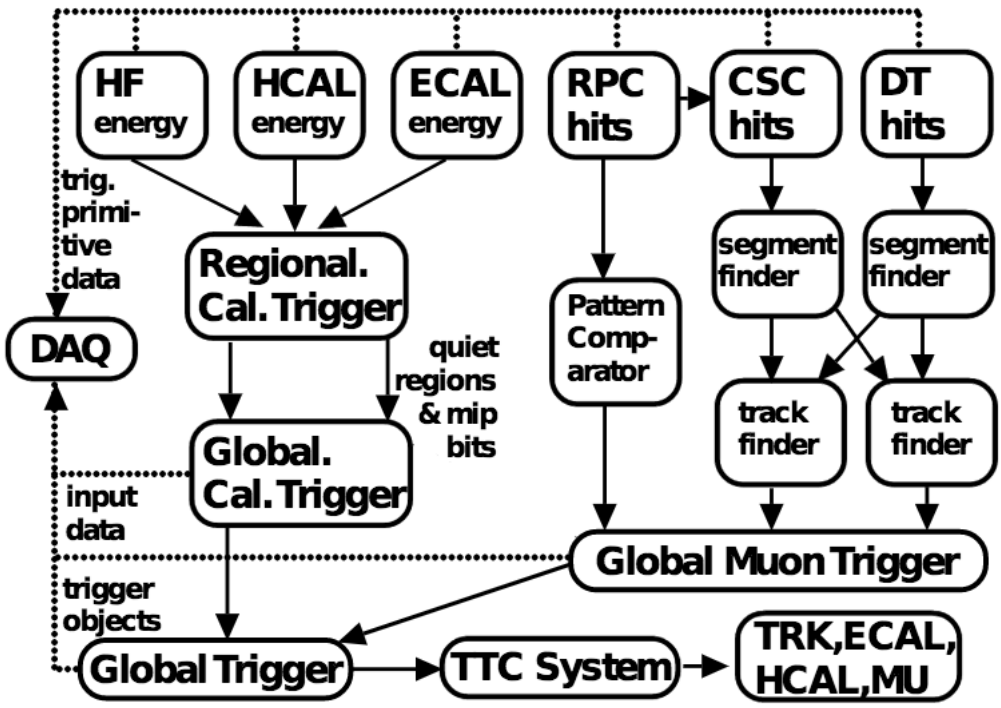

Figure 5.1: Overview of the CMS level-1 trigger system [15].

5.1.2 Muon trigger system

All the muon chamber sections contribute to the muon trigger system. The muon chamber energy deposits, or hits, are sent to pattern comparator or to a segment and track finders.

The pattern comparator identifies muon candidates and sends the information to the global muon trigger. The candidates are sent with a value of transverse momentum and a quality code together with information about the position of the hit in the muon system.

After that the information goes to a global muon trigger. The global muon trigger recognises whether the same muon candidate has been detected in multiple muon systems and merges these observations. The merging can be done geometrically. After this the information is sent to the GT where the candidates can be discarded by their quality or if they are reconstructed by only one track finder.

5.1.3 Global trigger system

The information from the global calorimeter and global muon triggers is then combined and the GT makes the final trigger decision. The GT either rejects or accepts

a physics event.

The GT chooses the events by demanding a threshold of for example energy or momentum, or demanding a certain position in the detector. The GT can also accept events based on the difference of position of two particles. The conditions can be combined with logic statements (AND-OR-NOT) to form up to 128 algorithms. These algorithms form the Level-1 menu.

The decision is then passed to the tracker, ECAL, HCAL and the muon systems. The information is also sent to the data acquisition system (DAQ), which reads data from subsystems for offline storage. The DAQ is then used by the HLT.

5.2 High level trigger system

The HLT is implemented in software and consists of a single processor farm and an event filter farm. At the HLT, physics objects are identified and selection criteria are applied in multiple steps. This happens by using layers of algorithms. The HLT reduces the rate from 100 kHz to 400 Hz.

Together with the Level-1 information the HLT makes the object identification. The PF-algorithm plays an important role and for example the missing transverse momentum is calculated at the HLT. Some objects need multiple steps at the HLT. This way the objects can be identified and constrained.

When triggering muons the HLT uses information from two levels called the Level-2 and Level-3 triggers. The Level-2 algorithm uses information from the muon system and the level-3 combines the information from the muon subdetectors with the tracker. The Level-3 defines also a local isolation variable to use isolation criteria.

Tau leptons are identified in three steps called Level-2, Level-2.5 and Level-3. The Level-2 tau trigger is based on the calorimeter information so only p_T thresholds can be applied. The Level-2.5 step consists of isolation with the information from the pixel detector. Finally the Level-3 uses the particle-flow algorithm to construct the object. The event reconstruction and the particle-flow algorithm is discussed in more detail in Section 6.1.

Events, that are accepted by the HLT, are sent to a software process, called the storage manager, and written on external disc. From there data is moved to the CMS Tier-0 computing center for permanent storage.

6. Charged Higgs boson analysis in the fully hadronic final state

The analysis used in this Thesis searches for the charged Higgs boson with the $H^{\pm} \to \tau^{\pm}\nu_{\tau}$ decay mode in the fully hadronic final state [14]. In this Chapter we will describe the tools used in the analysis.

If the charged Higgs boson exists, it would cause additional sources of tau leptons in the data compared to the prediction of the SM, as the charged Higgs boson could decay into $\tau\nu$ channel. Tau lepton decays into hadronic channels are chosen. Hadronically decaying tau lepton is denoted as τ_h.

The only neutrino in the event originates from the charged Higgs boson decay. This neutrino can be detected by measuring the missing transverse energy of the event. Since there appears only one neutrino in the event, by measuring the energies of the τ and $E_{\mathrm{T}}^{\mathrm{miss}}$ in the event we can calculate the charged Higgs boson transverse mass with

$$m_{\mathrm{T}} = \sqrt{2E_{\mathrm{T}}^{\tau\ \mathrm{jet}} E_{\mathrm{T}}^{\mathrm{miss}}(1 - \cos\Delta\phi)}, \tag{6.1}$$

where $\Delta\phi$ is the angle between the selected τ and $E_{\mathrm{T}}^{\mathrm{miss}}$ directions in the transverse plane. This variable can be used to extract limits, plots that exclude areas in the mass range. The analysis is still blinded so that the observed limits can't be seen in the limit plots and tables. This makes sure that the analysis is not changed to certain desired direction.

6.1 Event reconstruction

The collider events are reconstructed using particle-flow (PF) algorithm [16]. It combines information from the parts of the detector and identifies and reconstructs individual electrons, photons, muons, charged and neutral hadrons. The energy deposits, or hits, in the calorimeters and the tracker system are used as elements

which are linked with algorithms to blocks. With the blocks the PF algorithm reconstructs the physical objects.

Electrons are reconstructed by combining information from the tracker and the ECAL. The hits of the ECAL are fitted and compared with the data to construct the block. Photons can be reconstructed from the ECAL. If the ECAL hit is not linked with a track the block is considered as a photon. The ECAL hits are also compared to HCAL hits to make sure that the photon candidate is not really a hadron.

In the PF algorithm muons can be reconstructed from hits in the tracker and in the muon chambers. Selection criteria are applied to reduce misidentification. The tracks are then fitted to find the momentum of the particle.

If ECAL and HCAL hits are linked to tracks, the candidates are considered as charged hadrons. Generally hadrons leave some energy to the ECAL as well. The tracks in the tracker system distinguishes the charged and neutral hadrons.

Jets are reconstructed by using an anti-k_T algorithm [5] which is implemented in `FastJet` [6], which clusters hadrons and photons to form jets. Jets originating from b-quarks can be distinquished by using the Combined Secondary Vertex b-tagging algorithm [17]. Hadronically decaying tau leptons can be reconstructed with hadrons-plus-strip algorithm [18] by first combining the PF objets and then by identifying the source of the hadronic tau.

Primary vertex can be reconstructed by using deterministic annealing method [40]. The missing transverse momentum can be reconstructed by taking the negative vector sum of momenta of all PF particles in a event and taking a projection of it onto the plane perpendicular to the beams.

6.2 Tau plus E_T^{miss} trigger

The trigger of the analysis is designed to select events where a charged Higgs boson decays into a hadronic tau. The tau and missing transverse momentum (MET) triggers give the best efficiencies so they are used in the analysis to reduce the rate of undesired events.

The efficiencies of the tau and E_T^{miss} parts are measured separately as they are assumed to be uncorrelated. The triggers are used as an online selection having a 50 GeV threshold for taus and $|\eta| < 2.1$. For MET a threshold of 80 GeV is demanded at Level-1 and a threshold of 90 GeV is demanded at HLT.

The trigger efficiencies are then calculated for the data and simulations separately. The efficiencies are estimated in bins as a function of transverse momentum for the

tau part and as a function of missing transverse energy for the MET part of the trigger. The statistical errors in the efficiencies are considered for each bin separately. Scale factors are then used as a correction to match the simulation to data. The statistical uncertainties in the efficiency bins are passed to the scale factors and the uncertainty is then used as a systematical error in the analysis.

6.3 Event selection

After the trigger selection the events are still dominated by the backgrounds. To extract the signal events from the backgrounds, an event selection is used. The event selection designed to suppress the backgrounds is

- The primary vertex is the one with largest $\sum_i^{tracks} \mathrm{p}_\mathrm{T}^2$.
- One or more tau lepton with $\mathrm{p_T} > 50$ GeV, $|\eta| < 2.1$, leading track $\mathrm{p_T} > 30$. Isolation is also required.
- 3 or more hadronic jets with $\mathrm{p_T} > 30$ GeV $|\eta| < 4.7$. $\Delta R(\mathrm{jet}, \tau_h) > 0.5$.
- Electron veto with $\mathrm{p_T} > 15$ GeV and $|\eta| < 2.5$. Isolation is required.
- Missing transverse energy MET > 90 GeV.
- Muon veto with $\mathrm{p_T} > 10$ GeV and $|\eta| < 2.5$. Isolation is required.
- One or more b-tagged b-jet with $|\eta| < 2.5$.
- Angular cut $R_{\mathrm{bb}}^{\mathrm{min}} = \mathrm{min}\sqrt{(180^\circ - \Delta\phi(\tau, E_\mathrm{T}^{miss}))^2 + \Delta\phi(\mathrm{jet}, E_\mathrm{T}^{miss})^2} > 40^\circ$. Here we sum over the three jets in the event.

where η is the pseudorapidity, a variable that represents the place of a particle in the detector $\eta = -\ln(\tan(\frac{\theta}{2}))$, where θ is the angle between the three-momentum and the beam axis. The variable $\Delta R = \sqrt{(\Delta\phi)^2 + (\Delta\eta)^2}$ describes the distance of two objects in the ϕ, η plane.

The angular cuts in $R_{\mathrm{bb}}^{\mathrm{min}}$ are required to suppress multijet events. Events with electrons and muons satisfying the previous conditions are excluded. This allows us to select the fully hadronic final state.

6.4 Backgrounds

The main backgrounds of the analysis are QCD multijet events, electroweak (EWK)+$t\bar{t}$ events with a genuine tau and EWK+$t\bar{t}$ events with a fake tau. Fake taus are electrons, muons or hadronic jets that are misidentified as tau leptons. The EWK processes include W+jets, single Z/γ^* and diboson (WW,WZ,ZZ) production.

The QCD multijet and EWK+$t\bar{t}$ fake tau backgrounds are measured from data using inverted tau isolation [38]. The fake tau background is measured from a control region. As the isolation criteria of the taus suppresses the background significantly one can obtain a sample dominated by fake taus by rejecting events with at least one tau passing the isolation criteria. Other selection criteria is still applied.

The EWK+$t\bar{t}$ with genuine tau background is estimated from simulations. The estimation is done by applying full event selection on the simulated events. If a simulated tau is found within $\Delta R < 0.1$ on the reconstructed tau, the event is considered as a genuine tau event. If a simulated electron or muon is found in $\Delta R < 1$ the event is considered to be in the EWK+$t\bar{t}$ with fake tau. If no match is found for the tau jet, it is considered to come from a hadronic jet.

6.5 Systematic uncertainties of the analysis

In the analysis there appear multiple sources of systematical uncertainties. They are all presented in this subsection. We'll focus more in the scale factor uncertainties of the tau plus MET trigger.

6.5.1 Scale factor uncertainties

The scale factors of the tau plus MET trigger are defined as the ratio of efficiencies

$$SF = \frac{\epsilon_{\text{data}}}{\epsilon_{\text{MC}}}. \tag{6.2}$$

The scale factor uncertainties are defined at each point by varying the scale factor with respect to the efficiency uncertainties.

$$SF_{\text{vary data}} = \frac{\epsilon_{\text{data}} + \sigma^{\text{data}}_{\text{up}}}{\epsilon_{\text{MC}}}, \frac{\epsilon_{\text{data}} - \sigma^{\text{data}}_{\text{down}}}{\epsilon_{\text{MC}}} \tag{6.3}$$

$$SF_{\text{vary MC}} = \frac{\epsilon_{\text{data}}}{\epsilon_{\text{MC}} + \sigma^{\text{MC}}_{\text{up}}}, \frac{\epsilon_{\text{data}}}{\epsilon_{\text{MC}} - \sigma^{\text{MC}}_{\text{down}}} \tag{6.4}$$

where the uncertainty $\sigma^{MC/data}$ is the uncertainty assigned to MC or data respectively. Smaller statistical uncertainties in the efficiencies result in smaller uncertainties in the scale factors. These varied uncertainties are used as the up and down uncertainties of the scale factors for data and MC respectively.

The uncertainties are then passed as so called shape systematics to the analysis. These shapes are used in the final parts of the analysis, where the histograms are allowed to vary with respect to the shape systematics.

6.5.2 Additional sources of uncertainties

There appear also other scale factors and other sources of systematical uncertainties. In addition to the trigger uncertainties, there are

- Tau identification uncertainties
- Tau, jet and MET energy scale uncertainties
- Lepton veto uncertainties
- B-tagging uncertainties
- Top p_T reweighting uncertainties
- Cross section uncertainties
- Pileup reweighting uncertainties
- Luminosity uncertainties

To take into account the uncertainties in the tau identification, a 10 % uncertainty is applied. For large tau transverse momentum values a $20\% * p_T/1\text{TeV}$ uncertainty is associated. The uncertainty in the energy scale of hadronic taus is 3 % and uncertainties in jet energy scale and unclustered MET energy scale are calculated by shifting the energy scales. These are then propagated to the final distribution. Cross sections are allowed to vary within the theoretical uncertainties. The uncertainty in luminosity is 6.2 %.

All the systematic uncertainties of the final m_{T} distribution are summarised in Table 6.1. One can see that the systematical uncertainty in simulated part of the MET trigger is the dominant uncertainty of the analysis.

Table 6.1: The systematic uncertainties (in %) for the signal and the backgrounds. The uncertainties, which depend on the final distribution bin, are marked with (S) and for them the maximum contracted value of the negative or positive variation is displayed.

	Signal	Fake tau	EWK+$\bar{\mathrm{t}}\mathrm{t}$ genuine tau		
			$\bar{\mathrm{t}}\mathrm{t}$	W+jets	DY
tau ID	10	1.7	10	10	10
high-p_T tau ID (S)	0.4..15	< 0.1	< 0.1	0.3	0.6
trigger tau leg eff. for data (S)	3.6..16	0.8	2.9	3.6	4.0
trigger tau leg eff. for MC (S)	0.3..3.7	0.9	3.3	3.3	3.1
trigger MET leg eff. for data (S)	14..26	3.9	14	16	14
trigger MET leg eff. for MC (S)	0.6..1.7	0.3	1.1	1.0	1.2
electron veto eff.	0.3	–	0.3	< 0.1	0.3
muon veto eff.	0.2	–	0.2	< 0.1	0.3
b-tagging eff. (S)	4.5..7.2	1.1	5.7	0.3	1.3
b-mistagging eff. (S)	3.1..8.4	2.3	6.7	12	12
tau energy scale (S)	0.1..4.8	1.0	5.7	5.4	3.5
jet energy scale (S)	1.6..7.0	0.4	1.8	4.3	6.4
MET unclustered energy scale (S)	$< 0.1..0.5$	< 0.1	< 0.1	< 0.1	< 0.1
jet energy resolution (S)	0.3..2.5	0.2	< 0.1	6.2	3.2
top p_T reweighting (S)	–	1.4	8.1	–	–
pileup reweighting	5.0	5.0	5.0	5.0	5.0
ttbar scale	–	$^{+0.4}_{-0.6}$	$^{+2.4}_{-3.5}$	–	–
ttbar pdf	–	0.7	4.2	–	–
ttbar mass	–	0.5	2.8	–	–
W+jets scale	–	–	–	$^{+0.8}_{-0.4}$	–
W+jets pdf	–	–	–	3.8	–
DY scale	–	–	–	–	$^{+0.7}_{-0.4}$
DY pdf	–	–	–	–	3.7
diboson scale	–	–	–	–	–
diboson pdf	–	–	–	–	–
luminosity (13 TeV)	6.2	1.0	6.2	6.2	6.2
Fake tau template fit	–	–	–	–	–
Fake tau MET shape (S)	–	–	–	–	–

7. Fitting trigger efficiency to reduce systematic uncertainties

As described, in the analysis the trigger scale factors are estimated as a function of tau p_T or E_T^{miss} in bins. The uncertainties of these scale factors dominate the systematic uncertainties of the entire analysis. In this Chapter, we introduce a new method which fits the efficiencies as a function of p_T or E_T^{miss} and the uncertainties of the fit parameters are passed to the scale factors which are then used as systematic uncertainties in the analysis. We refer to the old method as "bin-by-bin method" and to the new method as a "fitting method".

7.1 Fitting method implementation

The efficiency calculation can be performed with a χ^2-fit or with a binned maximum likelihood fit. The χ^2-fit is at the moment not recommended to this analysis as fully working minimisation of χ^2-value requires large N and m and also large N-m values for efficiencies $\epsilon = \frac{m}{N}$. Here m is the amount of passed particles and N is the amount of considered events. At the moment the requirement of large m is not fulfilled in every bin. If these requirements are not achieved the result is biased due to finite bin size. The method is still implemented for possible future usage.

The binned maximum likelihood fit works well with finite bin sizes but is vulnerable to bins with very low statistics. This is not a problem in the current analysis, since the efficiencies don't have many bins with zero values. The fitting and error analysis here is based on [20].

The efficiency turn-on curve is theoretically described with a step function, where the step begins at the desired trigger threshold. In reality, the effects of ineffective resolution smear the turn-on in a way that it is best described by a curve.

To take this into account, four different functions are implemented to find the best

fit for the turn-on: the Sigmoid function

$$f_S = \frac{p_0}{1 + exp(-p_1(x - p_2))}, \tag{7.1}$$

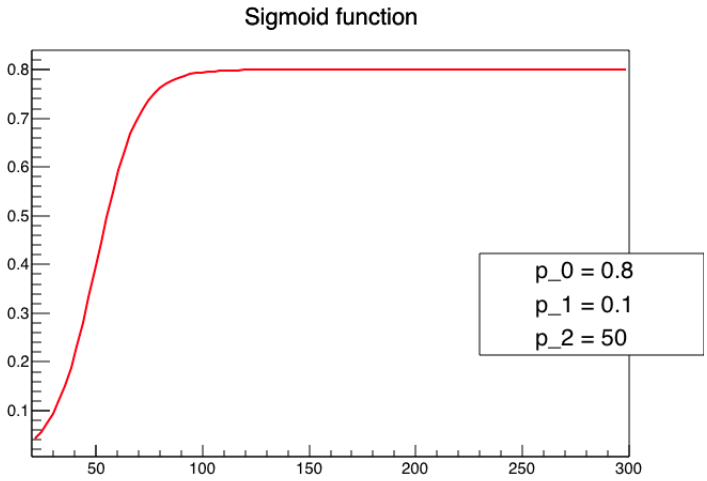

Figure 7.1: Illustrative figure of the Sigmoid function for set of parameters.

the Error function

$$f_E = \frac{1}{2} p_0 (1 + Erf((\sqrt{x} - \sqrt{p_1})/p_2)), \tag{7.2}$$

where Erf is the error function.

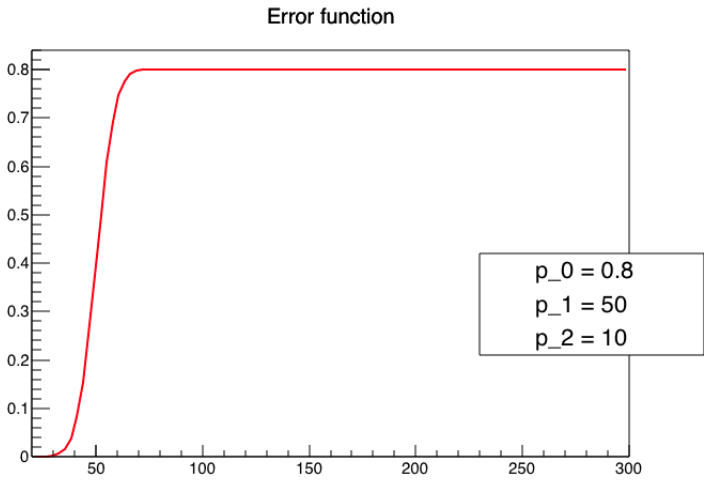

Figure 7.2: Illustrative figure of the Error function for set of parameters.

The Gompertz function

$$f_G = p_2 \left(\frac{1}{2}\right)^{(exp(-p_0(x-p_1)))}, \tag{7.3}$$

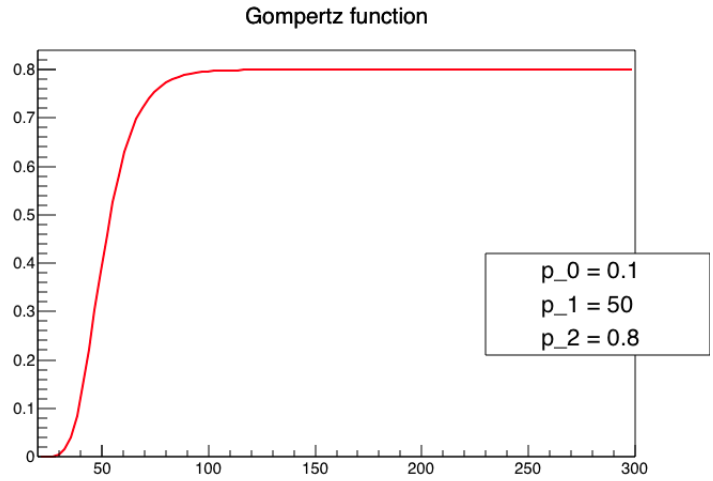

Figure 7.3: Illustrative figure of the Gompertz function for set of parameters.

the Richards function

$$f_R = \frac{p_2}{((1 + (2^{p_3} - 1)exp(-p_0(x - p_1)))^{1/p_3})} \tag{7.4}$$

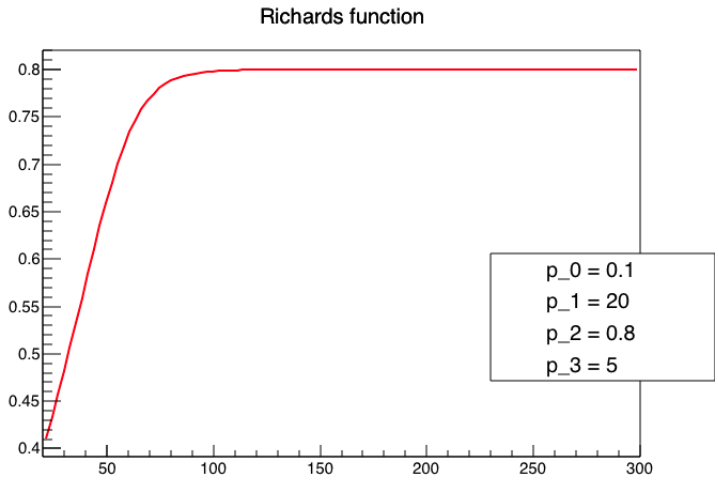

Figure 7.4: Illustrative figure of the Richards function for set of parameters.

and the cumulative distribution function of the crystal ball function. The crystal ball function is defined as

$$f_{CB} = N \begin{cases} exp(-\frac{(x-\bar{x})^2}{2\sigma^2}), & \text{for } \frac{(x-\bar{x})}{2\sigma} > -\alpha \\ A(B - \frac{(x-\bar{x})}{\sigma})^{-n}, & \text{for } \frac{(x-\bar{x})}{2\sigma} \leq -\alpha \end{cases} \tag{7.5}$$

where

$$A = (\frac{n}{|\alpha|})^n exp(-\frac{|\alpha|^2}{2}), \tag{7.6}$$

$$B = \frac{n}{|\alpha|} - |\alpha|, \tag{7.7}$$

$$N = \frac{1}{\sigma(C+D)}, \tag{7.8}$$

$$C = \frac{n}{|\alpha|}\frac{1}{n-1}exp(-\frac{|\alpha|^2}{2}), \tag{7.9}$$

$$D = \sqrt{\frac{\pi}{2}}1 + Erf(\frac{|\alpha|}{\sqrt{2}})) \tag{7.10}$$

and the cumulative distribution function can then be calculated as

$$f_C(x) = \int_{-\infty}^{x} f_{CB}dx' \tag{7.11}$$

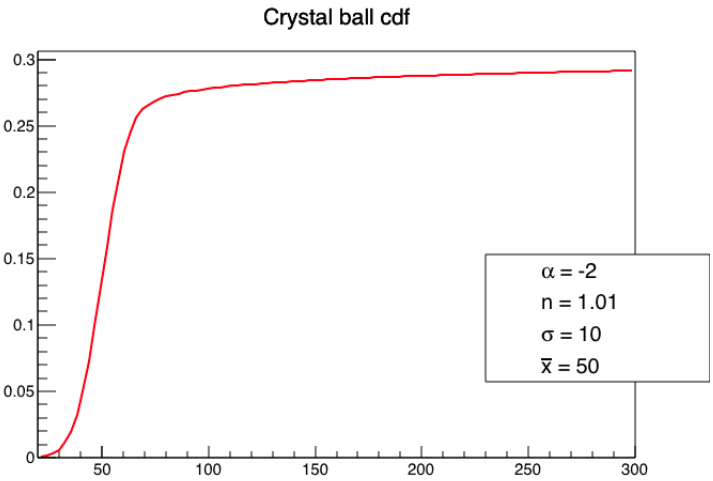

Figure 7.5: Illustrative figure of the Crystal ball cumulative distribution function for set of parameters.

In the functions p are the free fit parameters. In the crystal ball function the free parameters are denoted as α, n, σ and $\bar{x}$.

The bin-by-bin method suffers from the finite bin size also in a way how the information was passed on in the analysis. The bin-by-bin method was forced to pass the efficiencies in large steps required by the statistics. This way the function describing the efficiency is not accurate. This has been improved with the fitting method. After the fit, the efficiencies are passed on in 1 GeV steps giving more accurate description.

7.2 Uncertainty calculation

After performing the fit, the fitting method calculates the uncertainties of the fit parameters. The final uncertainties are then calculated using the standard error propagation taking into account the correlation between the fit parameters

$$\sigma_f = \sqrt{\sum_{ij} \frac{\partial f}{\partial \theta_i} \frac{\partial f}{\partial \theta_j} cov(\theta_i, \theta_j)}, \tag{7.12}$$

where the $cov(\theta_i, \theta_j)$ stands for the covariance matrix elements. Now the uncertainties of the fit parameters can be propagated as the uncertainty of the fit at each point: the Equation 7.12 gives a function of p_T or MET which can be added or subtracted from the fit at each point of p_T or MET. As described, the scale factors, used to scale the simulation to data, take the uncertainties of the efficiencies which are then considered as a systematical uncertainty in the analysis.

8. Results

The fitting method, for calculating the trigger efficiency scale factors, was developed for the charged Higgs boson analysis. The goal was to reduce systematical uncertainties in the scale factors by taking into account all the values of the efficiency. This would in turn reduce the systematical uncertainties of the whole analysis as the uncertainties in the MET part of the trigger dominated the old analysis. The new uncertainties were included in the analysis and the limits were calculated for the charged Higgs boson production to the fully hadronic final state.

8.1 Comparison of the two methods

New efficiencies of the data and simulation for the tau and the MET part of the analysis were fitted. The best fits were found to be Sigmoid functions for the tau part of the trigger. The fits best describing the MET part of the trigger were found to be the Crystal ball cumulative distribution for the data and the Richards function for the simulation. The chosen fits gave the best goodness of fit parameters $\chi^2/n.d.f$ together with the best description of the data and simulation points. For example, although the Richards function gave the best goodness of fit parameters for the tau part of the trigger it wasn't chosen as it did not describe the data and simulation points. This can be clearly seen from left subplot of Figure 8.4.

8.1.1 Efficiencies and scale factors

Here are presented all the fits made to the efficiencies using the method of maximum likelihood. The goodness of fit parameters are summarized in Table 8.1.

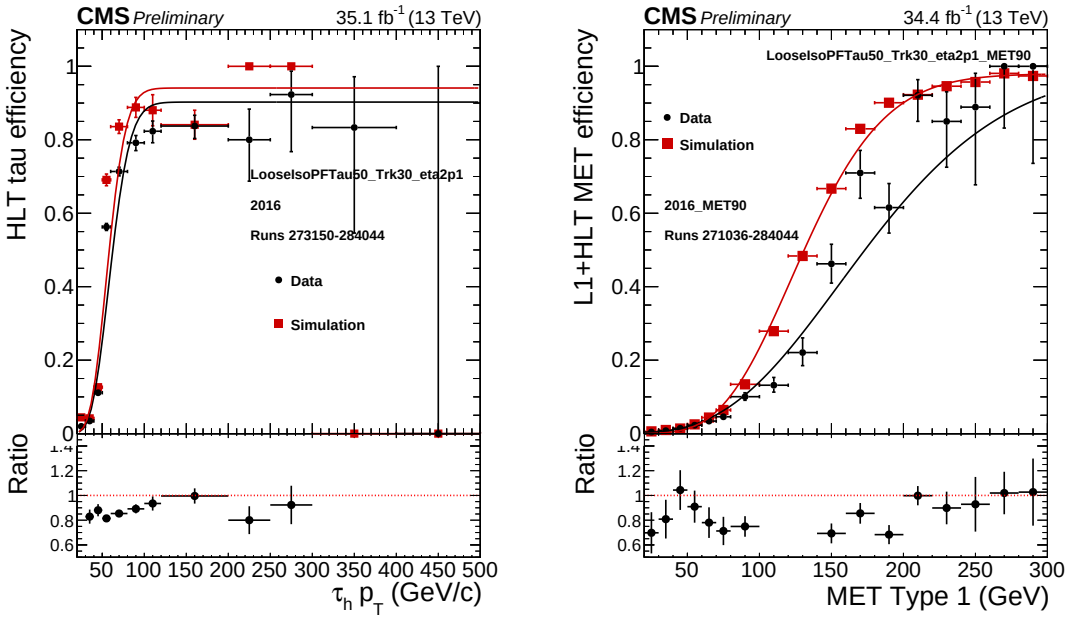

Figure 8.1: Tau and MET efficiencies for bin-by-bin method and for fitting method in black for data and in red for simulation. Fitted with the Error function.

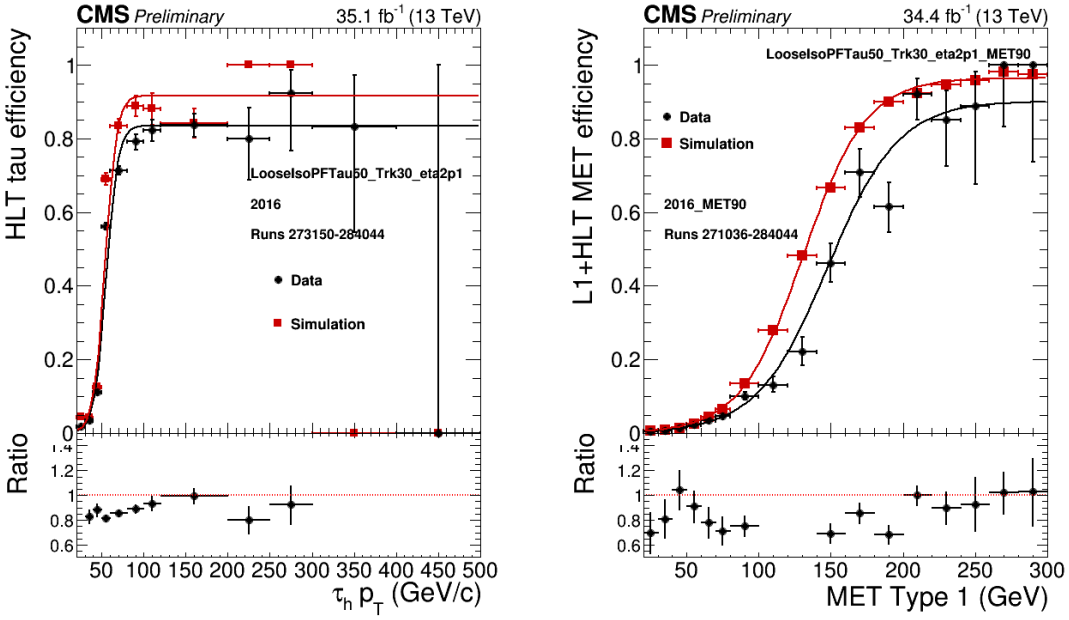

Figure 8.2: Tau and MET efficiencies for bin-by-bin method and for fitting method in black for data and in red for simulation. Fitted with the Sigmoid function.

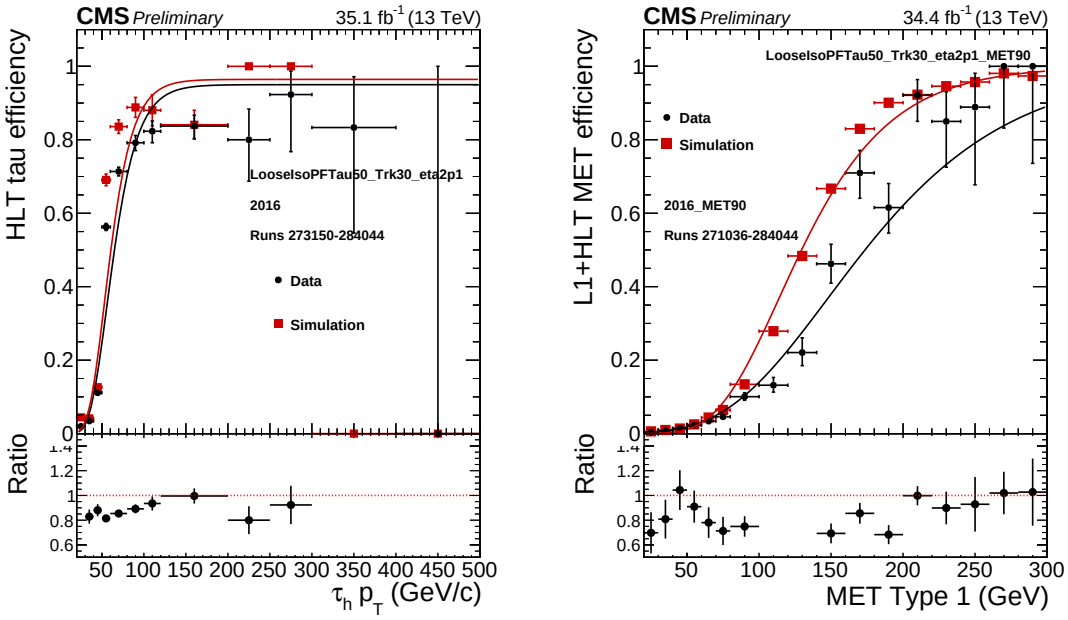

Figure 8.3: Tau and MET efficiencies for bin-by-bin method and for fitting method in black for data and in red for simulation. Fitted with the Gompertz function.

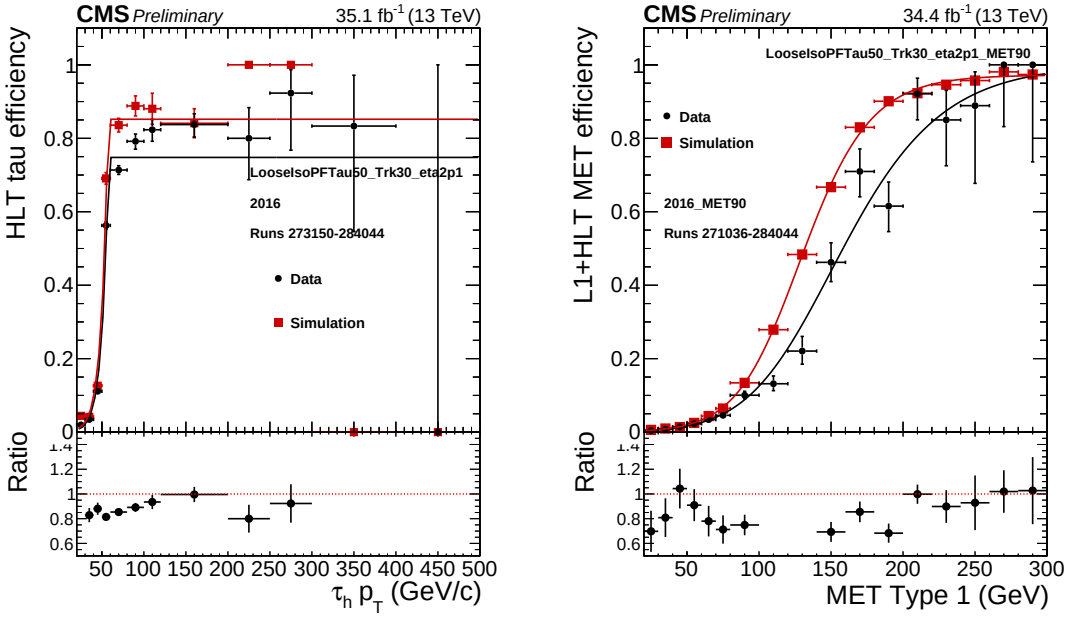

Figure 8.4: Tau and MET efficiencies for bin-by-bin method and for fitting method in black for data and in red for simulation. Fitted with the Richards function.

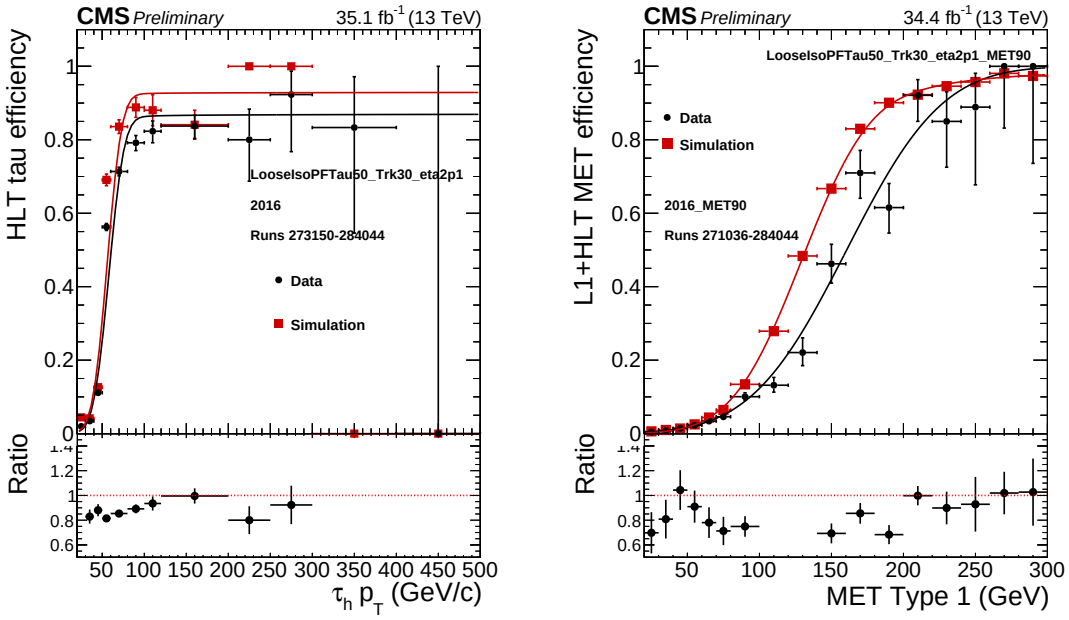

Figure 8.5: Tau and MET efficiencies for bin-by-bin method and for fitting method in black for data and in red for simulation. Fitted with the Crystal ball cumulative distribution function.

Table 8.1: $\chi^2/n.d.f$ values of the fits formatted in way that the best goodness of fit parameters are apparent.

Name	Fitted part			
	Tau data	Tau simulation	MET data	MET simulation
Error fuction	1416/(12-3)	817/(12-3)	62/(17-3)	1353/(17-3)
Sigmoid function	697/(12-3)	482/(12-3)	36/(17-3)	282/(17-3)
Gompertz function	1632/(12-3)	944/(12-3)	56/(17-3)	2435/(17-3)
Richards function	340/(12-4)	269/(12-4)	25/(17-4)	152/(17-4)
Crystal ball cdf	1065/(12-4)	653/(12-4)	22/(17-4)	232/(17-4)

The Table 8.1 illustrates the goodness of fit parameters of the fits. The $\chi^2/n.d.f$ values in the best case should be close to one. The $n.d.f$ value corresponds to number of points used in the fit subtracted by the number of fit parameters.

The value and statistical uncertainty of the fit parameters are shown in Table 8.2 for the tau part of the trigger and in Table 8.3 for MET part of the trigger.

Table 8.2: Sigmoid fit parameters and their absolute uncertainties for data (left) and simulation (right) for tau part of the trigger.

data parameter	value	uncertainty
p_1	0.835413	± 0.00962476
p_2	0.14306	± 0.00202364
p_3	55.4772	± 0.279442

simulation parameter	value	uncertainty
p_1	0.91749	± 0.0114134
p_2	0.145893	± 0.0035784
p_3	54.2504	± 0.377239

Table 8.3: Fit parameters and their absolute uncertainties for Crystal ball cdf fit for data (left) and Richards function fit for simulation (right) for MET part of the trigger. Although the uncertainty is large in the α the shape of the function is not affected much.

data parameter	value	uncertainty
α	-5.49195	$\pm$ 671.565
n	1.66831	$\pm$ 4.75611
σ	52.2379	$\pm$ 1.30456
$\bar{x}$	160.597	$\pm$ 2.60274

simulation parameter	value	uncertainty
p_1	0.0392138	$\pm$ 0.0005663
p_2	130.407	$\pm$ 0.211577
p_3	0.972089	$\pm$ 0.0011817
p_4	0.708436	$\pm$ 0.0233257

The statistical uncertainties of the fit parameters are then propagated to the total fit uncertainties as a function of $\mathrm{p_T}$ and MET. Then they are used to calculate the systematical uncertainties in the scale factors and finally in the m_T distribution.

8.1.2 Systematical uncertainties

The final systematical uncertainties of both bin-by-bin and fitting method are presented in Tables 8.4 and 8.5 for light charged Higgs boson for different backgrounds. For the heavy charged Higgs boson the uncertainties are presented in Tables 8.6 and 8.7. There always appears four scale factors as the scale factors are allowed to vary separately with respect to data or simulation efficiencies.

Table 8.4: The light charged Higgs boson systematic uncertainties (in %) for the bin-by-bin method. The uncertainties depend on the final distribution bin, so the maximum contracted value of the negative or positive variation is displayed.

	Signal	Fake tau	EWK+$\mathrm{t\bar{t}}$ genuine tau		
			$\mathrm{t\bar{t}}$	W+jets	DY
trigger tau leg eff. for data	2.5..4.1	0.4	2.6	3.2	3.6
trigger tau leg eff. for MC	3.0..4.5	0.5	3.1	3.2	3.0
trigger MET leg eff. for data	13..14	2.2	14	15	14
trigger MET leg eff. for MC	1.4..3.0	0.2	1.3	1.1	1.5

Table 8.5: The light charged Higgs boson systematic uncertainties (in %) for the fitting method. The uncertainties, which depend on the final distribution bin, so the maximum contracted value of the negative or positive variation is displayed.

	Signal	Fake tau	EWK+$t\bar{t}$ genuine tau		
			$t\bar{t}$	W+jets	DY
trigger tau leg eff. for data (S)	1.2..2.8	0.2	1.2	1.2	1.2
trigger tau leg eff. for MC (S)	1.5..3.1	0.3	1.6	1.5	1.4
trigger MET leg eff. for data (S)	3.3..4.9	0.5	2.9	2.4	3.2
trigger MET leg eff. for MC (S)	0.3..2.0	< 0.1	0.3	0.2	0.3

Table 8.6: The heavy charged Higgs boson systematic uncertainties (in %) for the bin-by-bin method, for trigger scale factors. The uncertainties, so the maximum contracted value of the negative or positive variation is displayed.

	Signal	Fake tau	EWK+$t\bar{t}$ genuine tau		
			$t\bar{t}$	W+jets	DY
trigger tau leg eff. for data	3.6..16	0.8	2.9	3.6	4.0
trigger tau leg eff. for simulation	0.3..3.7	0.9	3.3	3.3	3.1
trigger MET leg eff. for data	14..26	3.9	14	16	14
trigger MET leg eff. for simulation	0.6..1.7	0.3	1.1	1.0	1.2

Table 8.7: The heavy charged Higgs boson systematic uncertainties (in %) for the fitting method, for trigger scale factors. The uncertainties, so the maximum contracted value of the negative or positive variation is displayed.

	Signal	Fake tau	EWK+$t\bar{t}$ genuine tau		
			$t\bar{t}$	W+jets	DY
trigger tau leg eff. for data	1.1..1.6	0.3	1.1	1.1	1.1
trigger tau leg eff. for simulation	1.3..1.8	0.3	1.3	1.3	1.3
trigger MET leg eff. for data	0.2..3.6	0.7	2.9	2.3	3.0
trigger MET leg eff. for simulation	0.1..0.8	< 0.1	0.3	0.2	0.3

The Tables 8.4 and 8.5 show that the systematic uncertainties of the light mass region get smaller with the fitting method. Also the Tables 8.6 and 8.7 show that the systematic uncertainties of the heavy mass region are reduced with the fitting method.

The total systematical uncertainties are also shown in Figures 8.6 for the bin-by-bin method and in Figure 8.7 for the fitting method. One can see that the total

systematical uncertainties in the number of signal events is reduced with the fitting method.

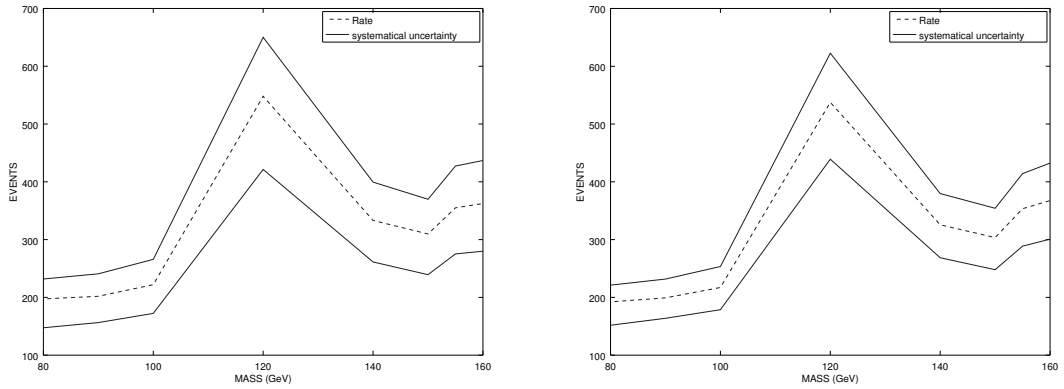

Figure 8.6: Total systematical uncertainties of the signal for the light charged Higgs boson for the bin-by-bin method (left) and for the fitting method (right).

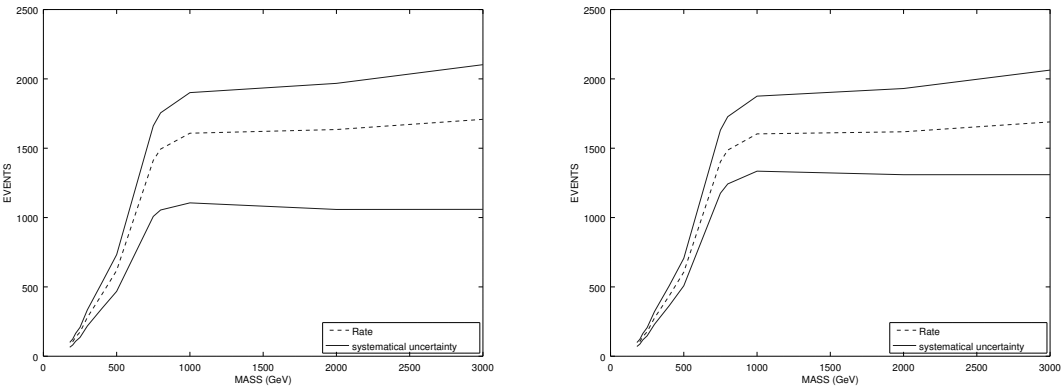

Figure 8.7: Total systematical uncertainties of the signal for the heavy charged Higgs boson for the bin-by-bin method (left) and for the fitting method (right).

8.1.3 Limits

The calculated limits for the charged Higgs boson production rate are presented. The limit calculation is based on the modified frequentist criterion [39] with a test statistics based on the profile likelihood ratio.

The limits are presented in Figure 8.8 for the light mass region and the values are also collected in the tables 8.8 and 8.9. The figures and tables compare the values given by the bin-by-bin method and the fitting method.

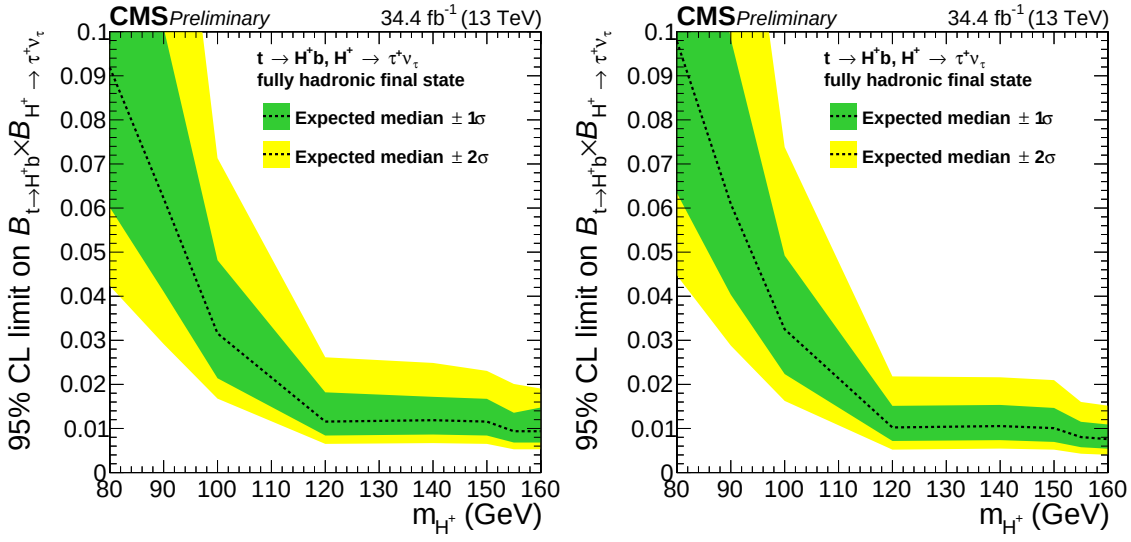

Figure 8.8: Limits for the light charged Higgs boson with the bin-by-bin method (left) and fitting method (right).

Table 8.8: Limits for the light charged Higgs boson with the bin-by-bin method.

95% CL upper limit on $B_{t\to H^+b} \times B_{H^+\to\tau\nu}$						
m_{H^+}	Expected limit					Observed
(GeV)	-2σ	-1σ	median	$+1\sigma$	$+2\sigma$	limit
80	0.04235	0.06015	0.09188	0.15193	0.27739	Blinded
90	0.02915	0.04102	0.06219	0.10086	0.17325	Blinded
100	0.01677	0.02139	0.03156	0.04817	0.07133	Blinded
120	0.00650	0.00840	0.01156	0.01820	0.02615	Blinded
140	0.00668	0.00863	0.01187	0.01718	0.02487	Blinded
150	0.00650	0.00840	0.01156	0.01672	0.02306	Blinded
155	0.00527	0.00681	0.00938	0.01356	0.02010	Blinded
160	0.00527	0.00681	0.00938	0.01476	0.01905	Blinded

Table 8.9: Limits for the light charged Higgs boson with the fitting method.

95% CL upper limit on $B_{t\to H^+b} \times B_{H^+\to\tau\nu}$						
m_{H^+}	Expected limit					Observed
(GeV)	-2σ	-1σ	median	$+1\sigma$	$+2\sigma$	limit
80	0.04470	0.06337	0.09781	0.16565	0.29640	Blinded
90	0.02880	0.04035	0.06094	0.09834	0.16356	Blinded
100	0.01625	0.02234	0.03250	0.04921	0.07383	Blinded
120	0.00520	0.00716	0.01023	0.01513	0.02181	Blinded
140	0.00544	0.00735	0.01055	0.01534	0.02161	Blinded
150	0.00520	0.00695	0.01008	0.01466	0.02097	Blinded
155	0.00427	0.00575	0.00805	0.01151	0.01602	Blinded
160	0.00403	0.00541	0.00758	0.01090	0.01517	Blinded

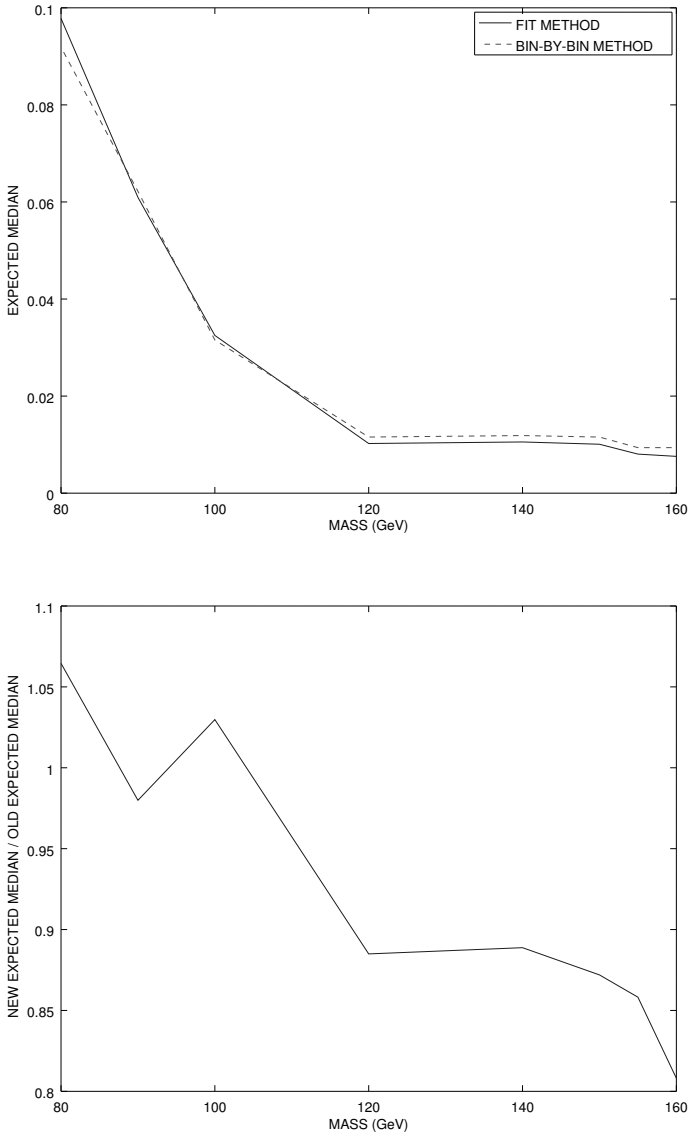

Figure 8.9: Expected medians of the bin-by-bin and fitting methods (top) and the ratio of the expected medians (bottom) for the light mass region.

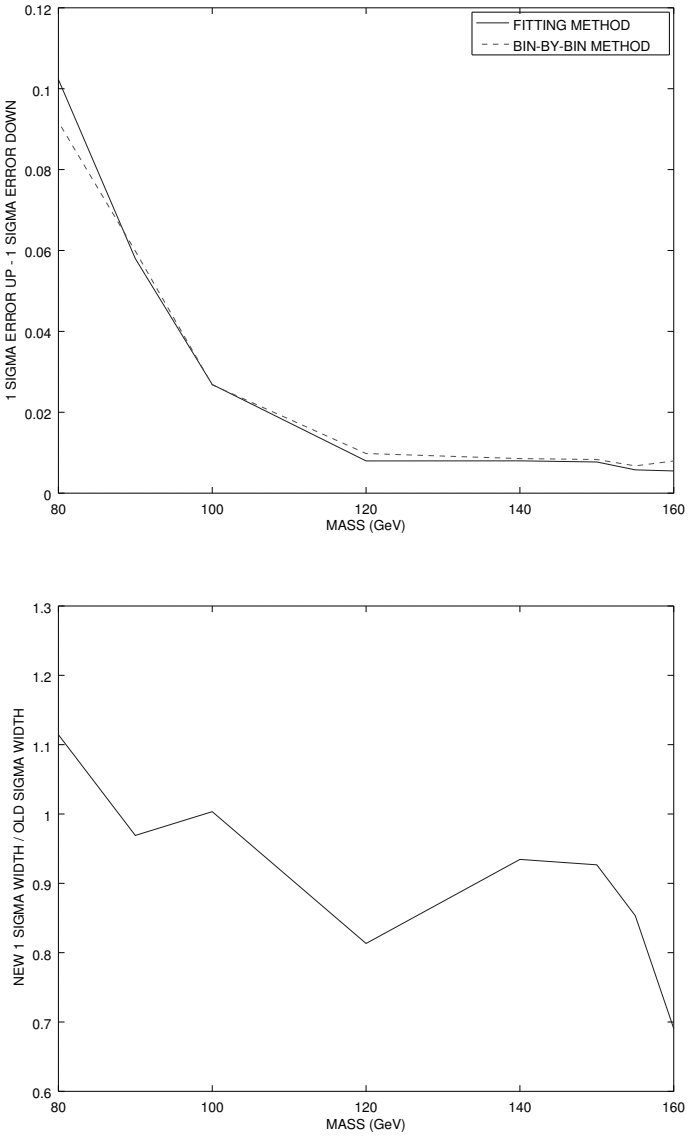

Figure 8.10: 1 σ confidence interval width of the bin-by-bin and fitting methods (top) and the ratio of the widths (bottom) for the light mass region.

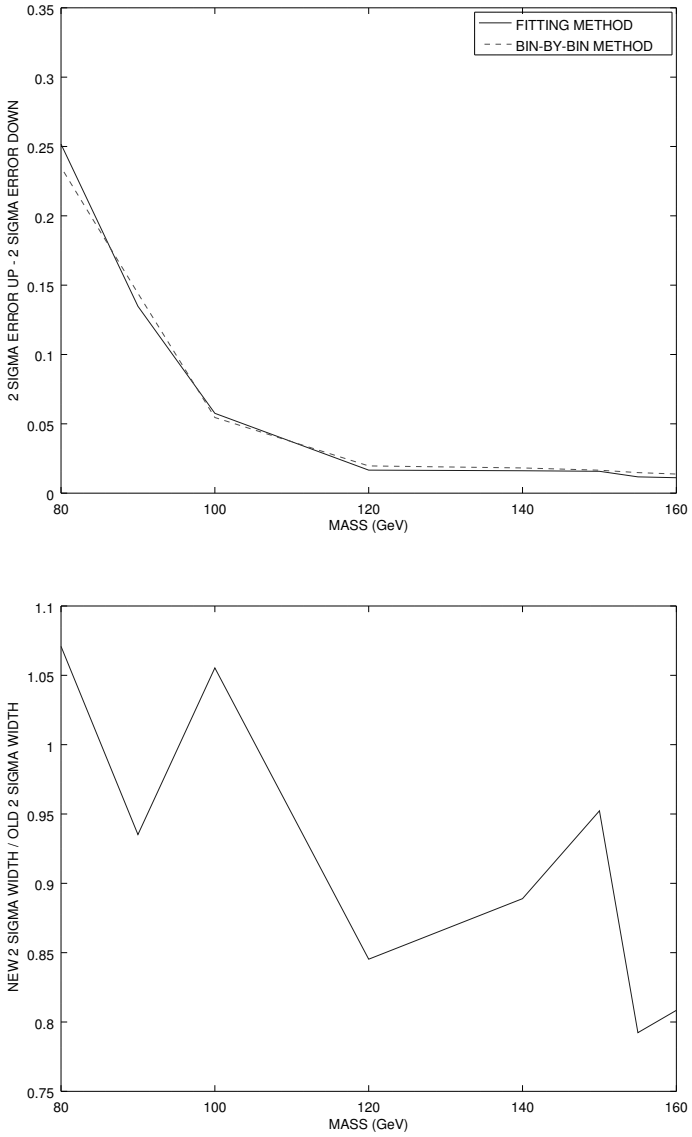

Figure 8.11: 2 σ confidence interval width of the bin-by-bin and fitting methods (top) and the ratio of the widths (bottom) for the light mass region.

The expected limits for the light mass region improve slightly by using the fitting method as can be seen from Figure 8.9. The uncertainty of the limits fluctuates, but is smaller for the fitting method for major parts of the light mass region as presented in Figures 8.10 and 8.11.

The limits for the heavy mass region are presented in Figure 8.12. The values are collected in the Tables 8.10 and 8.11.

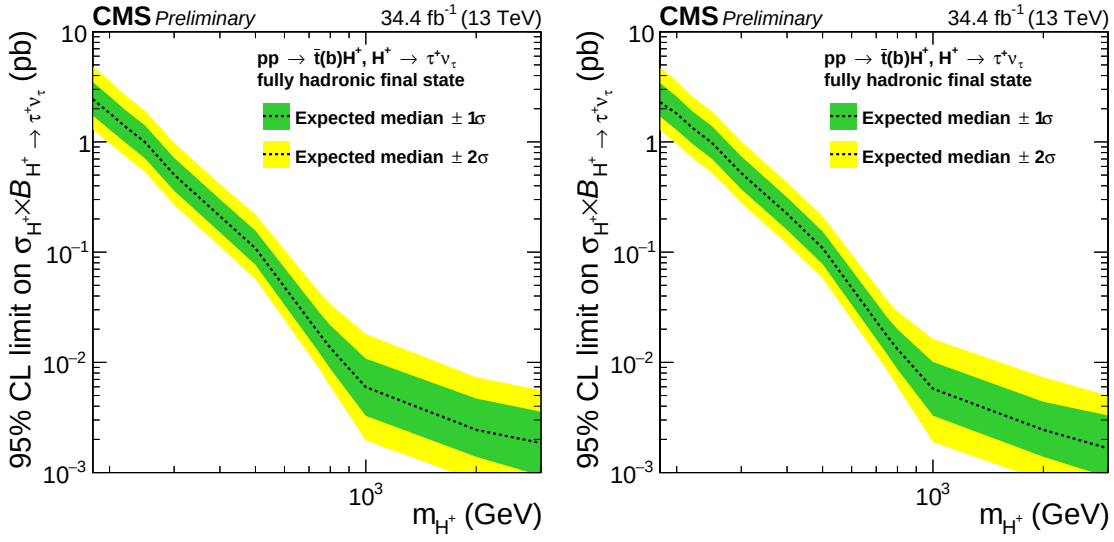

Figure 8.12: Limits for the heavy charged Higgs boson with the bin-by-bin method (left) and fitting method (right).

Table 8.10: Limits for the heavy charged Higgs boson with the bin-by-bin method.

95% CL upper limit on $\sigma_{H^+} \times B_{H^+ \to \tau\nu}$						
m_{H^+} (GeV)	Expected limit					Observed limit
	-2σ	-1σ	median	$+1\sigma$	$+2\sigma$	
180	1.29824	1.73676	2.44375	3.49577	4.83316	Blinded
200	0.96953	1.29702	1.82500	2.60337	3.60462	Blinded
220	0.74420	0.99671	1.39062	1.96711	2.68268	Blinded
250	0.53181	0.70865	0.99375	1.40967	1.91977	Blinded
300	0.26812	0.36053	0.50469	0.71793	0.98273	Blinded
400	0.11248	0.15124	0.21172	0.30202	0.41417	Blinded
500	0.05684	0.07665	0.10859	0.15664	0.21970	Blinded
750	0.00852	0.01195	0.01787	0.02792	0.04257	Blinded
800	0.00604	0.00875	0.01357	0.02169	0.03378	Blinded
1000	0.00195	0.00327	0.00596	0.01080	0.01806	Blinded
2000	0.00084	0.00139	0.00244	0.00470	0.00734	Blinded
3000	0.00052	0.00094	0.00186	0.00357	0.00558	Blinded

Table 8.11: Limits for the heavy charged Higgs boson with the fitting method.

95% CL upper limit on $\sigma_{Hplus} \times B_{\mathrm{H}^+ \to \tau\nu}$						
m_{H^+} (GeV)	Expected limit					Observed limit
	-2σ	-1σ	median	$+1\sigma$	$+2\sigma$	
180	1.27578	1.70787	2.30000	3.42765	4.75109	Blinded
200	0.95957	1.28369	1.80625	2.57663	3.56758	Blinded
220	0.72051	0.96884	1.35625	1.91308	2.61268	Blinded
250	0.52178	0.69882	0.97500	1.38307	1.88355	Blinded
300	0.27928	0.37215	0.52188	0.74030	1.00818	Blinded
400	0.11829	0.15906	0.22266	0.31407	0.42892	Blinded
500	0.05790	0.07785	0.10898	0.15460	0.21192	Blinded
750	0.00844	0.01183	0.01729	0.02562	0.03646	Blinded
800	0.00603	0.00865	0.01318	0.01996	0.02900	Blinded
1000	0.00189	0.00328	0.00576	0.01008	0.01630	Blinded
2000	0.00084	0.00139	0.00244	0.00439	0.00733	Blinded
3000	0.00057	0.00091	0.00166	0.00330	0.00499	Blinded

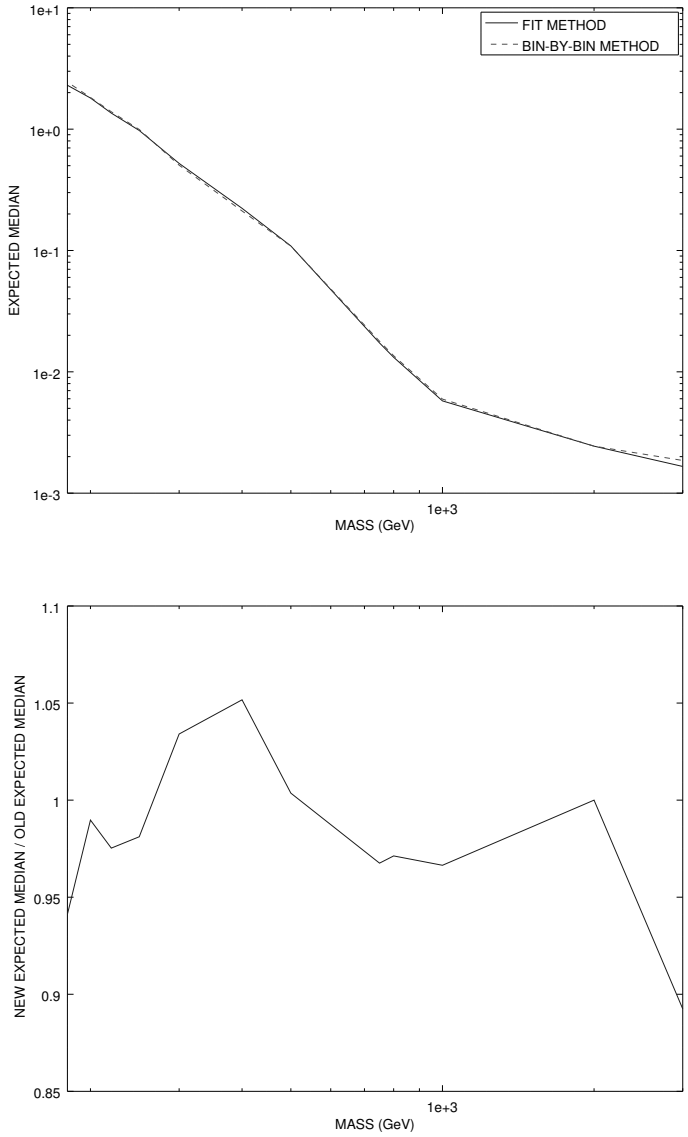

Figure 8.13: Expected medians of the bin-by-bin and fitting methods (top) and the ratio of the expected medians (bottom) for the heavy mass region.

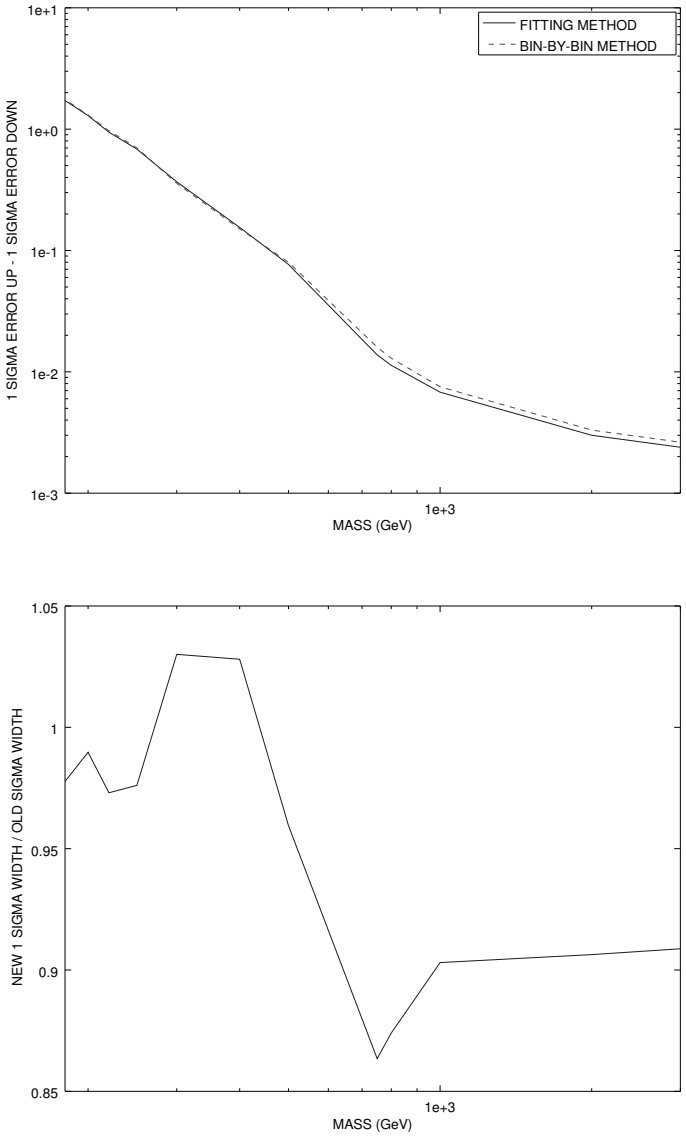

Figure 8.14: 1 σ confidence interval width of the bin-by-bin and fitting methods (top) and the ratio of the widths (bottom) for the heavy mass region.

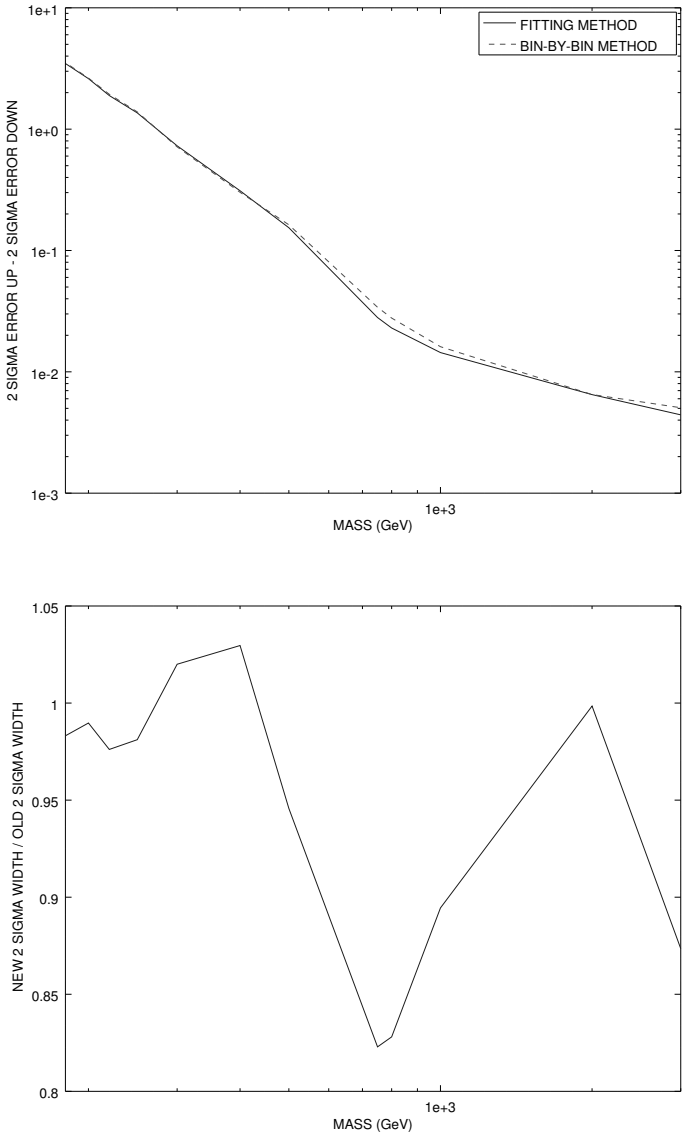

Figure 8.15: 2 σ confidence interval width of the bin-by-bin and fitting methods (top) and the ratio of the widths (bottom) for the heavy mass region.

The expected limits for the heavy mass region improve only little with the fitting method as illustrated in Figure 8.13. The fitting method gives slightly larger uncertainties around 400 GeV but smaller uncertainties on other parts of the mass range as shown in Figures 8.14 and 8.15. The expected limits and the uncertainties don't change as much as in the light mass region.

9. Conclusions

The fitting method was developed for the charged Higgs boson analysis efficiency measurement. The goal was to reduce the systematical uncertainties in the scale factors. The systematical uncertainties of the scale factors are reduced with the fitting method significantly as can be seen from Tables 8.5 and 8.7. The MET uncertainty, which before was the dominant uncertainty, has been reduced from a maximum value of 20 % to a value of about 4 % for the heavy mass region. For the light mass region the scale factor uncertainty was reduced from 14 % to 5 %. Also the uncertainty in the tau part of the trigger was reduced. Changes in the final limits were compared. It seems that the reduction of systematical uncertainties in the scale factors doesn't straight forward mean that the final uncertainties in the limits get better.

The efficiency fits describe well the MET part of the trigger. This can be seen from an acceptable $\chi^2/n.d.f.$ value. The fits of the tau part of the trigger are not so good as the ratio of $\chi^2/n.d.f.$ is not optimal. The fluctuations in the measured efficiencies are so strong that the turn on curve doesn't seem to describe the efficiency. Bad fits may give underestimated statistical uncertainties for the fit parameters, which is good to keep in mind with the tau part of the trigger.

The fitting method makes large changes to the efficiency compared to the bin-by-bin method. Mainly the changes make efficiencies smaller compared to the bin-by-bin method on some regions. The efficiency plateau is smaller for the fitting method for the tau part of the trigger. The smaller plateau value makes the amount of signal events in the analysis smaller as the efficiency is smaller. This in turn can be seen as a slightly changed transverse mass distribution. It is also good to point out that although the uncertainties are smaller, the value of scale factors varies compared to the bin-by bin method.

The uncertainties of the light mass region limits are reduced with the fitting method. The expected limits also improve slightly. For the heavy mass region the uncertainties in the limits improve on some parts of the mass range. The light mass range limits show more improvement than the heavy mass range limits. The fact that the limits don't change significantly with decreasing systematical errors could indicate that the analysis might need more statistics in the heavy mass region.

Final conclusion is that it is beneficial to change the analysis to use the fitting method instead of the bin-by-bin method. It is good to keep in mind that the fits of the tau part of the trigger are not optimal and may result in underestimated uncertainties. With increasing statistics however the fitting method is expected to give better and more accurate results as the systematical uncertainties in the scale factors are smaller.

References

1 Charged Higgs boson branching ratio plots. https://twiki.cern.ch/twiki/bin/view/LHCPhysics/LHCHXSWGCrossSectionsFigures#H_BR_plots_MSSM, 2008. [Online; accessed 2017-09-27].

2 Georges Aad, B Abbott, J Abdallah, S Abdel Khalek, O Abdinov, R Aben, B Abi, M Abolins, OS AbouZeid, H Abramowicz, et al. Search for charged higgs bosons decaying via h±→ τ±ν in fully hadronic final states using pp collision data at s= 8 tev with the atlas detector. *Journal of high energy physics*, 2015(3):88, 2015.

3 J. Abdallah et al. Search for charged Higgs bosons at LEP in general two Higgs doublet models. *Eur. Phys. J.*, C34:399–418, 2004. doi:10.1140/epjc/s2004-01732-6.

4 W Bentz, IC Cloet, JT Londergan, and AW Thomas. Reassessment of the nutev determination of the weak mixing angle. *Physics Letters B*, 693(4):462–466, 2010.

5 Matteo Cacciari, Gavin P Salam, and Gregory Soyez. The anti-kt jet clustering algorithm. *Journal of High Energy Physics*, 2008(04):063, 2008.

6 Matteo Cacciari, Gavin P Salam, and Gregory Soyez. Fastjet user manual. *The European Physical Journal C*, 72(3):1896, 2012.

7 JW Christenson and VL Cronin. Fitch and r. turlay. *Phys. Rev. Letters*, 13:138, 1964.

8 ATLAS Collaboration. Observation of a new particle in the search for the standard model higgs boson with the atlas detector at the lhc. *Phys. Lett. B 716*, 2012.

9 CDF Collaboration. Search for charged higgs bosons from top quark decays in $p\overline{p}$ collisions at $\sqrt{s} = 1.96$ TeV. *Phys. Rev. Lett.*, 96:042003, Feb 2006. https://link.aps.org/doi/10.1103/PhysRevLett.96.042003, doi: 10.1103/PhysRevLett.96.042003.

10 CMS Collaboration. *CMS TriDAS project: Technical Design Report, Volume 1: The Trigger Systems*. Technical Design Report CMS. https://cds.cern.ch/record/706847.

11 CMS Collaboration. The CMS Experiment at the CERN LHC. *JINST*, 3:S08004, 2008. doi: 10.1088/1748-0221/3/08/S08004.

12 CMS Collaboration. Observation of a new boson at a mass of 125 gev with the cms experiment at the lhc. *Physics Letters B*, 716(1):30

– 61, 2012. http://www.sciencedirect.com/science/article/pii/S0370269312008581, doi: https://doi.org/10.1016/j.physletb.2012.08.021.

13 CMS Collaboration. Search for a charged higgs boson in pp collisions at $\sqrt{s}$= 8 tev. *Journal of High Energy Physics*, 2015(11):18, Nov 2015. https://doi.org/10.1007/JHEP11(2015)018, doi: 10.1007/JHEP11(2015)018.

14 CMS Collaboration. Search for charged Higgs bosons with the $H^{\pm} \to \tau^{\pm}\nu_{\tau}$ decay channel in the fully hadronic final state at $\sqrt{s} = 13$ TeV. Technical Report CMS-PAS-HIG-16-031, CERN, Geneva, 2016. https://cds.cern.ch/record/2223865.

15 CMS collaboration. The cms trigger system. *Journal of Instrumentation*, 12(01):P01020, 2017. http://stacks.iop.org/1748-0221/12/i=01/a=P01020.

16 CMS Collaboration. Particle-flow reconstruction and global event description with the cms detector. *JINST*, 12:P10003, 2017. doi: 10.1088/1748-0221/12/10/P10003, report: CMS-PRF-14-001, CERN-EP-2017-110.

17 CMS collaboration et al. Identification of b-quark jets with the cms experiment. *Journal of Instrumentation*, 8(04):P04013, 2013.

18 CMS collaboration et al. Reconstruction and identification of τ lepton decays to hadrons and $\nu\tau$ at cms. *Journal of Instrumentation*, 11(01):P01019, 2016.

19 D0 Collaboration. Search for charged higgs bosons in top quark decays. *Physics Letters B*, 682(3):278 – 286, 2009. http://www.sciencedirect.com/science/article/pii/S0370269309013495, doi: https://doi.org/10.1016/j.physletb.2009.11.016.

20 Glen Cowan. Error analysis for efficiency. *RHUL Physics, July*, 2008.

21 Siona Ruth Davis. Interactive Slice of the CMS detector. Aug 2016. https://cds.cern.ch/record/2205172.

22 Céline Degrande, Rikkert Frederix, Valentin Hirschi, Maria Ubiali, Marius Wiesemann, and Marco Zaro. Accurate predictions for charged higgs production: closing the mh± mt window. *Physics Letters B*, 2017.

23 Michael Dine, Willy Fischler, and Mark Srednicki. A simple solution to the strong cp problem with a harmless axion. *Physics letters B*, 104(3):199–202, 1981.

24 François Englert and Robert Brout. Broken symmetry and the mass of gauge vector mesons. *Physical Review Letters*, 13(9):321, 1964.

25 Lyndon Evans and Philip Bryant. Lhc machine. *Journal of Instrumentation*, 3(08):S08001, 2008.

26 Ludvig D Faddeev and Victor N Popov. Feynman diagrams for the yang-mills field. *Physics Letters B*, 25(1):29–30, 1967.

27 Pierre Fayet and J Iliopoulos. Spontaneously broken supergauge symmetries and goldstone spinors. *Physics Letters B*, 51(5):461–464, 1974.

28 Y Fukuda, T Hayakawa, E Ichihara, K Inoue, K Ishihara, H Ishino, Y Itow, T Kajita, J Kameda, S Kasuga, et al. Evidence for oscillation of atmospheric neutrinos. *Physical Review Letters*, 81(8):1562, 1998.

29 Jeffrey Goldstone, Abdus Salam, and Steven Weinberg. Broken symmetries. *Physical Review*, 127(3):965, 1962.

30 John F. Gunion and Howard E. Haber. Cp. *Phys. Rev. D*, 67:075019, Apr 2003. https://link.aps.org/doi/10.1103/PhysRevD.67.075019, doi: 10.1103/PhysRevD.67.075019.

31 Gerald S Guralnik, Carl R Hagen, and Thomas WB Kibble. Global conservation laws and massless particles. *Physical Review Letters*, 13(20):585, 1964.

32 Moo-Young Han and Yoichiro Nambu. Three-triplet model with double su (3) symmetry. *Physical Review*, 139(4B):B1006, 1965.

33 Robert Harlander, Michael Kramer, and Markus Schumacher. Bottom-quark associated Higgs-boson production: reconciling the four- and five-flavour scheme approach. 2011. report: CERN-PH-TH-2011-134, FR-PHENO-2011-009, TTK-11-17, WUB-11-04.

34 Peter W Higgs. Broken symmetries and the masses of gauge bosons. *Physical Review Letters*, 13(16):508, 1964.

35 T. D. Lee. A theory of spontaneous t violation. *Phys. Rev. D*, 8:1226–1239, Aug 1973. https://link.aps.org/doi/10.1103/PhysRevD.8.1226, doi: 10.1103/PhysRevD.8.1226.

36 Stephen P Martin. A supersymmetry primer. *Adv. Ser. Direct. High Energy Phys*, 21(515):1–153, 2010.

37 MissMJ. Standard Model of Elementary Particles. PBS NOVA, Fermilab, Office of Science, United States Department of Energy, Particle Data Group, 2006.

38 E. Pekkarinen. Data-driven measurement of the background with misidentified tau leptons in a search for charged higgs bosons. *g2 pro gradu, diplomityo*, 2015.

39 Alexander L Read. Presentation of search results: the cls technique. *Journal of Physics G: Nuclear and Particle Physics*, 28(10):2693, 2002.

40 Kenneth Rose. Deterministic annealing for clustering, compression, classification, regression, and related optimization problems. *Proceedings of the IEEE*, 86(11):2210–2239, 1998.

41 Tai Sakuma and Thomas McCauley. Detector and event visualization with SketchUp at the CMS experiment. Technical Report CMS-CR-2013-379. arXiv:1311.4942, CERN, Geneva, Oct 2013. https://cds.cern.ch/record/1626816, doi: 10.1088/1742-6596/513/2/022032.

42 Utpal Sarkar. *Particle and Astroparticle physics*. CRC Press, 2007.

43 Julius Wess and Bruno Zumino. Supergauge invariant extension of quantum electrodynamics. *Nuclear Physics B*, 78(1):1–13, 1974.

44 Julius Wess and Bruno Zumino. Supergauge transformations in four dimensions. *Nuclear Physics B*, 70(1):39–50, 1974.